UNIVERSITÀ DEGLI STUDI DI MILANO

DOTTORATO IN MEDICINA MOLECOLARE

E TRASLAZIONALE

CICLO XXX

Anno Accademico 2016/2017

TESI DI DOTTORATO DI RICERCA

MED/08

EXOSOMES SIGNALLING IN HUMAN GLIOMA STEM CELLS: THE CENTRAL ROLE OF V-ATPASE PROTON PUMP

Dottorando : Irene BERTOLINI

Matricola N° R10914

TUTORE : Prof. Stefano Ferrero

CO-TUTORE: Dott.ssa Valentina VAIRA

COORDINATORE DEL DOTTORATO: Prof. Riccardo GHIDONI

ABSTRACT

Recent evidences highlighted that glioblastomas (GBM) secreted microvesicles (EVs), particularly exosomes (Exo) and large oncosomes (LO), play a major role in the cross-talk between tumor cell and non-neoplastic parenchyma. Recent work from our group has identified the vacuolar pump H+-ATPase (V-ATPase) as an important effector of GBM growth and glioma stem cells (GSC) maintenance. Additionally, in ExoCarta database V-ATPase subunits have been described in Exo from different cancer cell types. Taken together, these data identify V-ATPase as an important driver of gliomagenesis, and a novel, actionable therapeutic target for disease intervention. However, the role of V-ATPase in reprogramming the GBM microenvironment has not been previously investigated. The aim of this project was investigate production, biological effect and content of extracellular vesicles according to proton pump activity in glioma stem cells.

Our data show that GSC are able to produce different types of EVs, which are internalized by recipient cells of different histology, such as non-neoplastic brain tumor margins, primary GBM monolayers (both differentiated and undifferentiated), and commercial glioma cultures. Exo and LO from GSC induces in recipient cells distinct effects. In particular, Exo significantly increased cell growth and cell motility, and these effects were stronger with Exo produced by NS with higher V-ATPase expression ($V1G1^{HIGH}$ NS). On the other hand, LO were able to strongly induce the sphere formation ability of primary GBM cultures. This effect lasted up 90 days after co-culture. In both situations, the block of V-ATPase activity by Bafilomycin A1 in NS-producing EVs completely reverted the effects.

Interestingly, exosomes are able to vehiculate on their surface the V-ATPase G1 subunit, and its protein level increased in recipient cells after co-culture with EVs. At the molecular level, profiling of Exo-derived miRNAs distinguishes $V1G1^{HIGH}$ NS from $V1G1^{LOW}$ cultures. In silico analysis and annotation of miRNA target genes showed an enrichment of cancer, cell cycle and MAPK/Erk pathways. Regarding signaling pathway modulation by Exo in recipient cells, exosomes from $V1G1^{HIGH}$ NS activated the MAPK/Erk pathway.

Altogether, these data point toward the central role of different EV types in GBM communication and suggest a role of the V-ATPase proton pump in regulating exosomes contents.

SOMMARIO

Evidenze recenti hanno dimostrato come nel glioblastoma le microvescicole (EVs), in particolare esosomi (Exo) e large oncosomes (LO), giochino un ruolo fondamentale nella comunicazione fra cellule tumorali e parenchima non-neoplastico. Un lavoro, pubblicato recentemente dal nostro gruppo di ricerca, ha identificato la pompa vacuolare H+-ATPase (V-ATPase) come un importante regolatore della crescita del glioblastoma e del mantenimento della nicchia di cellule staminali del glioma (GSC). Inoltre, nel database ExoCarta è riportato che diverse subunità della V-ATPase vengono veicolate negli esosomi derivanti da diversi tipi tumorali. Nell'insieme, questi dati identificano la V-ATPase come un importante regolatore dello sviluppo del GBM e come un nuovo possibile target terapeutico. Ad oggi però, il ruolo della V-ATPase nella regolazione del microambiente del GBM non è ancora stato studiato. Lo scopo di questo lavoro è stato quello di investigare la produzione, l'effetto biologico ed il contenuto delle microvescicole prodotte dalle GSC in accordo con l'espressione della pompa vacuolare.

In questo lavoro di tesi abbiamo dimostrato che le neurosfere (NS – cellule tumorali arricchite in GSC) sono in grado di produrre diversi tipi di microvescicole, le quali vengono internalizzate da cellule riceventi di diversa istologia, in particolare, margini tumorali celebrali non neoplastici, cellule primarie di glioblastoma (entrambe differenziate ed indifferenziate) e linee cellulari commerciali di glioma. Exo e LO sono in grado di produrre nelle cellule riceventi diversi effetti biologici. In particolare, gli Exo sono in grado di aumentare la crescita cellulare e la motilità, in entrambi casi l'effetto è maggiori in seguito a co-coltura con esosomi isolati da NS con alti livelli di V-ATPase ($V1G1^{HIGH}$ NS). D'altra parte, gli LO sono in grado di aumentare la capacità di cellule primarie di GBM di formare neurosfere; inducendo un effetto che si protrae fino a 90 giorni in coltura. In entrambi i casi, il blocco dell'attività della V-ATPase nelle NS che producono le EVs, con la Bafilomicina A1, è in grado di revertire completamente gli effetti.

È inoltre di interesse come gli esosomi prodotti dalle NS siano in grado di veicolare la subunità V1G1 sulla loro superficie, e di indurne l'espressione nelle cellule riceventi in seguito a co-coltura. A livello molecolare, il profilo dei miRNA isolati dagli esosomi è in grado di distinguere V1G1^{HIGH} NS da V1G1^{LOW}. Inoltre, studi in silico dei target dei miRNA differenzialmente espressi nei due gruppi di esosomi, mostrano un arricchimento in geni coinvolti in pathway tumorali, ciclo cellulare e MAPK/Erk pathway. In merito ai pathway modulati dagli esosomi nelle cellule riceventi, gli esosomi isolati da V1G1^{HIGH} NS sono in grado di attivare il pathway delle MAPK/Erk.

Nell'insieme questi dati supportano l'ipotesi che differenti tipi di microvescicole abbiano un ruolo centrale nel GBM nella comunicazione inter-cellulare e suggeriscono il ruolo della pompa protonica V-ATPase nel regolare il contenuto degli esosomi.

INDEX

1.INTRODUCTION

1.1 Human glioma

Adult diffuse gliomas are the most common tumor of the central nervous system (CNS), characterized by infiltrating growth, therapeutic resistance and aggressive nature. Untill 2007, the classification of brain tumor has been based on histological parameters, and they are subdivided into grades II-IV as oligodendroglioma, oligo-astrocytoma, astrocytoma and glioblastoma [1]. In 2016 WHO redefined the diffuse gliomas based also on the molecular parameters, in particular the recent glioma classification is based on the status of mutations of isocitrate dehydrogenase genes 1 and 2 (IDH1/2), 1p/19q co-deletion, ATRX alterations, and TERT promoter mutation status [2]. Moreover, glioma classification was restructured in order to consider all diffuse gliomas (astrocytomas and oligodendrogliomas) under the common header of “diffuse astrocytic and oligodendroglial tumors” [3], [4] (Fig.1).

Glioblastomas (GBM) have a high tendency for diffusely infiltrate the surrounding normal tissue, inducing malignant progression, that make them fatal. In 2016, in CNS World Health Organization (WHO), GBM were subdivided into glioblastomas IDH-wildtype (almost 90% of cases, corresponds, most frequently, to primary or de novo GBM) and IDH-mutant (about 10%, corresponds to secondary GBM). Despite large-scale genomic analyses of these tumors allowed the identification of mutations that drive tumor development and the collection of huge amount of data on brain tumors, the overall survival of GBM cases is still not that different than it was several years ago [5].

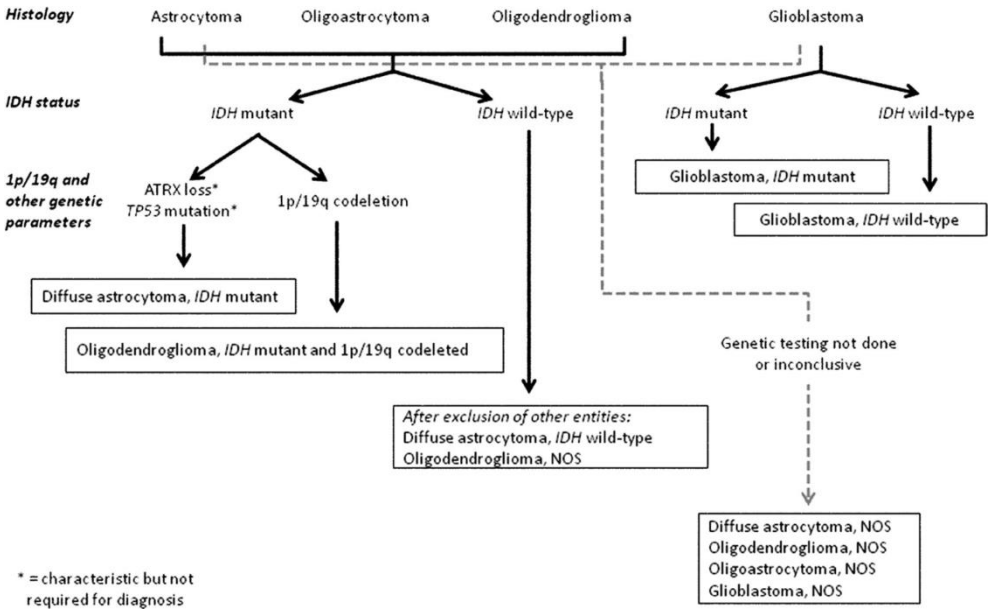

Fig.1_Classification of the diffuse gliomas based on histological and genetic features [4]. Captured by "The 2016 WHO classification of tumors of the CNV: a summary".

1.1.1. Brain tumor therapy

1.1.1.1 Glioma diagnosis

Patients with a malignant glioma may present a variety of symptoms including headache, confusion and loss of memory, neurological deficits and personality changes. The diagnosis of malignant gliomas is usually made by magnetic resonance imaging (MRI), computer tomography (CT) or positron emission tomography (PET). The images typically show an enhancing mass surrounded by edema. GBMs frequently have central areas of necrosis and more extensive peritumoral edema than those associated with anaplastic gliomas [6], [7].

1.1.1.2. Glioma prognosis

Life expectancy for glioma patients has not improved considerably and is only about 2-3 years for anaplastic astrocytoma and 15 months for GBM [6]. There are several reasons why it has been so difficult to find new

effective therapies against glioma. First, drug delivery is limited by the blood-brain-barrier impediment and the distorted glioma vessels [8]. Second, the invasive nature of gliomas makes the complete surgical resection of the tumor impossible. Third, tumor cells also have a strong intrinsic attitude for malignant progression and some cells, supposedly the cancer stem cells, are resistant to therapy. Lastly, over-expression of proteins involved in DNA repair machinery could dampen the effects of radio- and chemotherapy [9].

1.1.1.3 Treatment

The standard treatment for gliomas is the surgical resection, radiotherapy and chemotherapy using alkylating agents. The size and localization of the tumor is important for the possibility to perform optimal surgery. Due to their invasive growth, gliomas indeed are impossible to completely resect. Surgical elimination of the tumor reduces the symptoms caused by mass effect and seems to give a modest survival advantage to the patient. For patients with GBM, the median survival from time of diagnosis is about three months without treatment. After treatment with surgery and postoperative temozolomide and radiotherapy, the survival increases to 14.6 months [6]. O-6-methylguanine-DNA methyltransferase (MGMT) is an important repair enzyme that contributes to resistance to temozolomide. Methylation of MGMT promoter silences the gene, decreasing DNA repair activity and increasing the susceptibility of the tumor cells to temozolomide. Treatment with temozolomide in GBM patients with MGMT promoter methylation prolonged the survival to 2 years [10].

1.1.2 Glioma stem cells

Growing evidence indicates that rare population of cancer cells, called glioma stem cells (GSC), play a central role in driving invasive brain tumor growth and relapse [11]. Interestingly, GSCs are not spread evenly in tumor, but are enriched in tumor areas characterized by necrotic foci

surrounded by severely hypoxic pseudo-palisading cells. The presence of tumor necrosis and hypoxia are believed to be responsible for the acidification of the cellular microenvironment and to favor invasion of the surrounding brain parenchyma by glioma cells [12], [13]. In addition, hypoxia and acidification of tumor microenvironment have been shown to elicit oncogenic signaling pathways fuel tumor cell migration, sustain the cancer-initiating cell niche [14], [15], [16].

Neuron cancer stem cells are expandable when placed in culture and stimulated with the appropriate growth factors, such as epidermal growth factor (EGF) and fibroblast growth factor 2 (FGF2) [17]. This neurospheres approach represents a serum-free, selective culture system in which most differentiated cells rapidly die, whereas neural stem cells respond to mitogens, divide and form neurospheres that can be dissociated and re-plated to generate secondary spheres (Fig.2). This methods allows expansion and identification of neural stem cells, and has become the method of choice to study potential expanded neural stem-cell populations in vitro. [18]

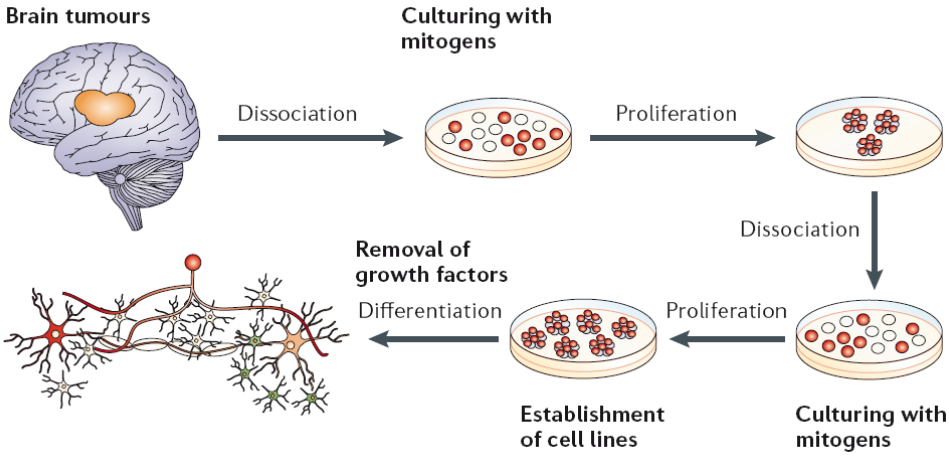

Fig.2_Cancer stem cells isolation from glioblastomas. Captured from "Brain tumour stem cells", Vescovi et al., Nature reviews, 2006. [17]

1.2 V-ATPase proton pump

V-ATPase is a ubiquitous multisubunit (up to 14) proton pump organized into two main domains (Fig.3). The V1 sector, a peripheral complex of 650 kDa, located on the cytoplasmic side of the membrane, that carries out ATP hydrolysis. Instead, the V0 domain, a membrane-embedded complex (260 kDa), is responsible for the translocation of protons. V1 sector is composed of eight different subunits (A, B1-B2, C1-C2, D, E1-E2, F, G1-G2-G3, H), whereas V0 contains six different subunits (a1-a2-a3-a4, d1-d2, e, c, and c″) [19], [20], [21].

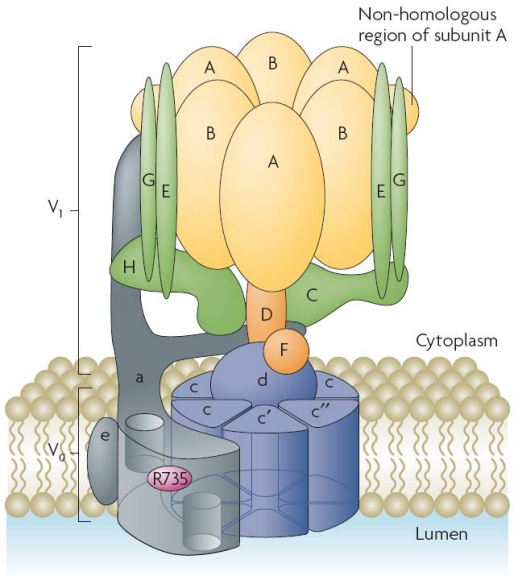

Fig.3_V-ATPase proton pump. Captured from "Vacuolar ATPases: rotary proton pumps in physiology and pathophysiology", Forgac, Nature reviews, 2007. [19]

V-ATPase may locate in different intracellular organelles (plasma membrane, lysosomes, endosomes, golgi and ER) and has various function both in physiological and pathological conditions. In particular is involved in the energization of transport processes across membranes and in the regulation of the intracellular or intraorganellar pH. Moreover contributes in endocytosis, invasion of tumor cells, angiogenesis and autophagy [22]. For example, in endosomes the V-ATPase pump, generating an acidic pH, allows the uncoupling of internalized ligand–receptor complexes and facilitates recycling of unoccupied receptors back to the cell surface. Moreover, proton pump has a central role in lysosomes, where the low pH is required by degradative enzymes to degrade internalized macromolecules. In secretory vesicles, V-ATPase established a proton potential gradients that drive the uptake of small molecules (Fig.4). Finally, the plasma membrane V-ATPase has important role in physiological process, such as renal acidificatiom, but is also implicated in

various human diseases, like cancer, where membrane V-ATPase has a central role in the survival and invasiveness of tumor cells [19], [23]. Finally, the V-ATPase has a central also in regulating intracellular pathways, in particular Wnt and Notch signaling [22], [24].

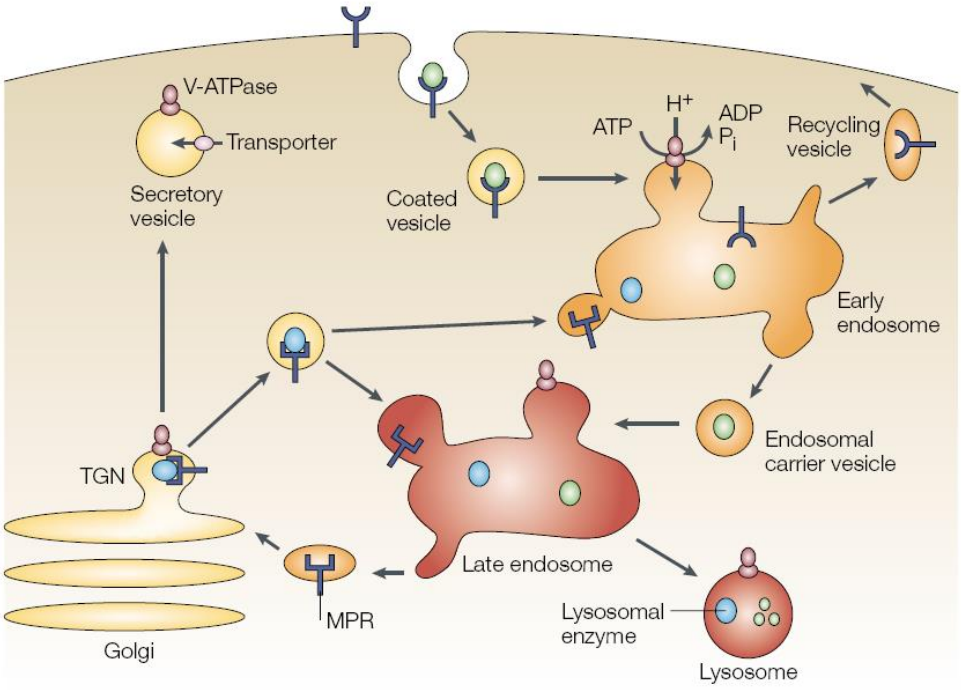

Figure 4_Role of intracellular V-ATPases in normal and disease processes. Captured from "The vacuolar (H+)-ATPases – nature's most versatile proton pumps", Tsuyoshi Nishi and Michael Forgac, Nature reviews, 2002 [25].

1.2.1 Specific inhibitors of the V-ATPases

The acidic extracellular mileu is one of the main traits of solid tumor and V-ATPase has a central role in this process. In theory, the inhibition of V-ATPase activity in cancer cells may suppress this acidification, that provides the necessary condition for tissue damage, inflammation and

degradation of ECM (extracellular matrix), and increase the survival rate of cancer patients [23].

The first V-ATPase inhibitors identified and structurally described, in the early 1980s, were Bafilomycin and Concanamycin (Fig. 5) [26], [27]. Bafilomycin A1 is a macrolide antibiotic derived from Streptomyces griseus, whereas Concanamycin was isolated from the culture medium of Streptomyces diastatochromogenes [28].

Was Bowman in 1988 that discovered Bafilomycin A1 as first highly specific V-ATPase inhibitors [29]; founding that it targets the V-ATPase V0 sector, inhibiting rotation and passage of protons into the lysosomal lumen, thereby reducing vesicle acidification. Subsequently, it was described that also Concanamycin is able to bind V0 sector and block V-ATPase activity at nano-concentrations [26].

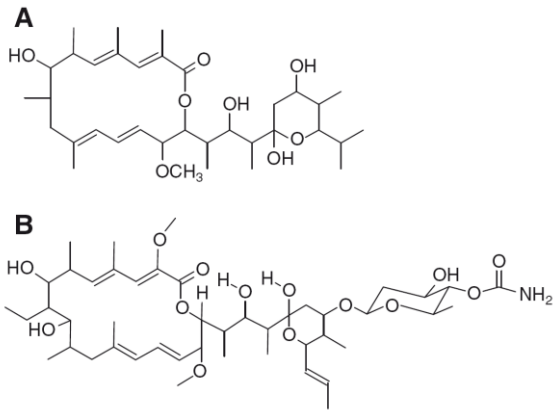

Fig.5_Bafilomycin A1 (A) and Concanamycin A (B) structure. Captured from “Inhibitors of V-ATPases: old and new players”, Huss et al., The Journal of Experimental Biology reviews, 2009 [27].

1.3 Extracellular vescicles

Extracellular vesicles (EVs) are naturally released membrane vesicles that can be classified into three main groups: exosomes (Exo), microvesicles (MVs) and apoptotic bodies (AB) [30], [31]. EVs are classified based on size, biological function and origin: Exo (40-200nm) are released from multivesicular bodies (MVB), MVs are produced directly from budding of plasma membrane (200-1000nm) and ABs are released by apoptotic cells (800-5000nm). Recently, was discovered an addition class of EVs, specifically produced by cancer cells, called large oncosomes (LO, 1000-10000nm) [32],[33] (Figure 6).

EVs can exert pleiotropic biological functions, and can influence the microenvironment via the horizontal transfer of bioactive molecules, signatures and genetic information to cells in their vicinity as well as distant sites. EVs have been implicated in several physiological and pathological processes, such as inflammation, immune disorders, neurological diseases, and cancer. Cancer EVs can act numerous functions, including regulating antitumor immunity, angiogenesis, drug resistance, metastasis and intercellular communication [34], [35].

In recent years, research on EVs has increased exponentially, yet few studies compared the content and biological effect of Exo and MVs produced by same types of cell. In fact, given that Exo and MVs have a different intracellular origins, they may have different function roles.

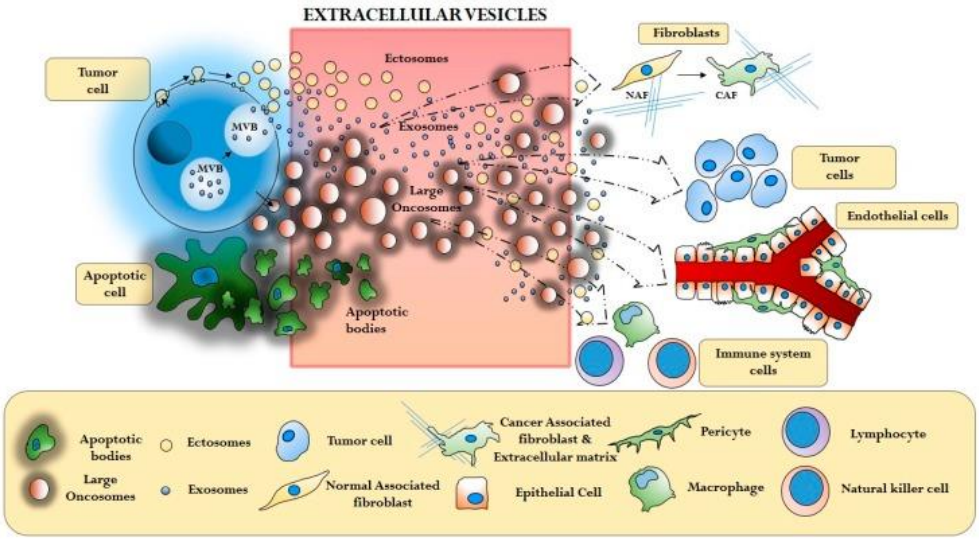

Fig. 6_Extracellular vesicles, interaction between cancer cells and tumor microenvironment. Captured from "Focus on Extracellular Vesicles: New Frontiers of Cell-to-Cell Communication in Cancer", Ciardiello et al., 2016, Int J Mol Sci. [35]

1.3.1 Large Oncosomes

Large oncosomes are a new class of EVs, described for the first time in 2008, as large vesicles produced by brain tumor cells able to vehiculate the oncogenic form of EGFR (variant III) [32]. Therefore, in 2009, Di Vizio described the production by metastatic prostate cancer cells of gigantic EVs (1-10um), produced directly from plasma membrane [33]. That giant vesicles were then called LO, because their atypically dimension and abundance of oncogenic cargo.

LO are originated directly from plasma membrane of highly migratory, aggressive tumor cells with an amoeboid phenotype. In particular, their production is associated to an overexpression of oncoproteins, such as MyrAkt1, HB-EGF, and caveolin-1 (Cav-1), or to an activation of the EGFR [33], [36].

Only tumor cells release LO at a quantifiable rate, and the number of large oncosomes is directly correlated with aggressiveness of tumor cells. LO vehiculate different types of bioactive molecules, including signaling factors involved in cell metabolism, mRNA processing and cell growth and motility. They also contain miRNAs and metalloproteinases [36], [37].

Given their recent discovery, few is known about LO and objective criteria of identification are necessary to obtain standardized procedures. Moreover, at that moment, we don't know much about a possible overlap in terms of molecular cargo and function between LO and MVs. Additional investigation is required not only to better define both large oncosome content and function in tumor progression but also to identify markers to determine if they represent a unique EV population.

1.3.2 Exosomes

Exosomes are nano-sized (40-200nm) vesicles that originated from the late endosomal trafficking machinery. Morphologically they appear as spherical structure, with a bilayer lipid membrane and sediment at 100.000g. Exosomes may vehiculate different types of lipid and protein on their membrane, and their composition depend on cell of origin. The most frequent protein present on exo-membrane are tetraspanin family members (CD9, CD63, CD81), ESCRT family member (Alix, Tsg101), enzymes involved in cell metabolism (Enolase1, Aldolase A,..), heat shock protein (Hsp70 and Hsp90) and small actin-binding protein (Cofilin1) [35], [38], [A, B,C].

Exosome formation starts at the surface where clathrin aggregates allow plasma membrane (PM) budding and the formation of clathrin-coated vesicles (CCVs) that following detachment and clathrin recycling become Early Endosomes (EEs). EE membrane undergoes structural rearrangements that ultimately lead to the inward invagination of the bilayer and the formation of ILVs in Late Endosome (LE) pouch that is hence

called MVB. MVB can become secretory, by fusion with the PM and release of its content in extracellular environment, or be fated to ultimate degradation by lysosome mediated processing (fig.7) [39], [40].

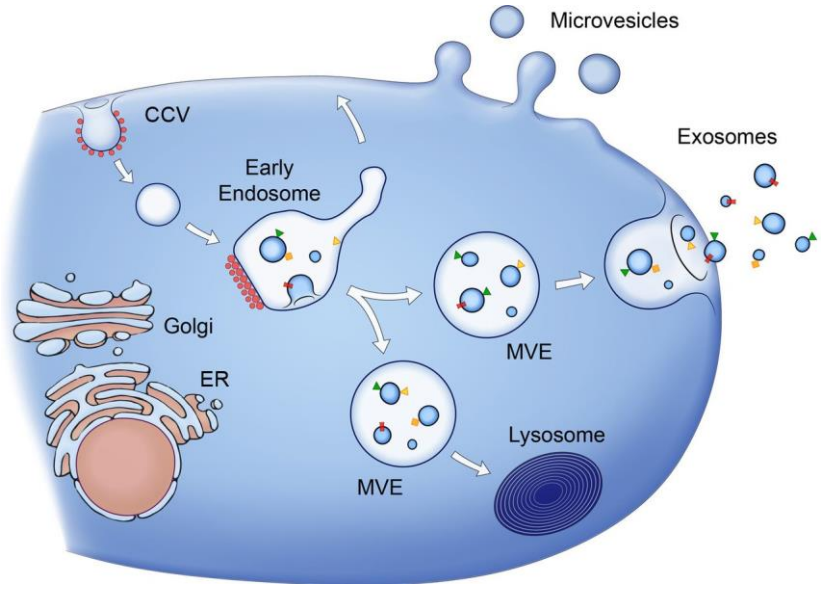

Fig.7_Exosomes biogenesis. Captured from "Extracellular vesicles: Exosomes, microvesicles, and friends", Raposo and Stoorvogel, JCB review, 2013 [39].

1.3.3 Extracellular vesicles in cancer

Today we know that cancer cells communicate also through EVs at a paracrine level, thanks the transferring of cargo molecules, proteins, lipids and RNAs, within the host. Cancer cells are able to produce different types of EVs that may influence different types of recipient cells, like endothelium cells, fibroblast, immune cells and other cancer cells [35], [41].

A variety of different study on EVs in cancer progression have been made in recent years and it was demonstrated that EVs vehiculate mutant and transforming protein and nucleic acid. For example EVs are able to transport mutant EGFR/EGFRvIII, MET, K-ras, H-ras and other oncoproteins. Moreover, are also able to transport tumor suppressor genes,

as PTEN, p53, DKK4 and miRNA, but also oncogenic transcripts and genomic DNAs [42], [43].

Tumor EVs regulate and participate in the dissemination of cancer cells, and recent evidence show how both tumor- and stroma-derived EVs are involved in the different steps of the metastatic cascade. For example it was demonstrated that EVs can alter the cellular physiology of both surrounding and distant non-tumor cells to allow dissemination and growth of cancer cells (by triggering vascular permeability or by conditioning pre-metastatic sites in distant organs) [38].

All together these studies demonstrate that EVs are involved in several aspect of tumor development and progression and their better study and characterization are required in order to use them both for diagnostic and therapeutic purpose.

1.3.4 miRNA in exosomes

The idea that miRNA secreted in EVs can be functionally delivered to target cells, resulting in direct modulation of their mRNA targets, has become one of the most actively explored hypotheses in the EV field, especially in cancer. In body fluids, miRNAs have been identified both within EVs and in complex with the argonaute RISC catalytic factor AGO2. Recent studies demonstrate that miRNA internalization in MVB is a fine-tuned process, depending on the miRNA sequence motif, cell type and physiological state [35], [44].

Different studies demonstrate that cancer exosomes vehiculate an higher number of miRNA compared to physiological condition, but recent evidence show that a decrease in tumor suppressor miRNA in exosomes might be a mechanism of pro-metastatic initiation [45]. Distinct patterns of miRNA expression have been observed in many cancers, including GBMs, and the functional significance of some of these miRNA alterations is beginning to emerge. Only recently, researchers have focused on the possible role of

miRNA in the microenvironmental communication of glioblastoma, primarily through the release and uptake of EVs. The analysis of EV/microRNA networks suggests that they can affect the tumor microenvironment in different ways: (i) direct reprogramming of cells in the tumor microenvironment (ii) indirect reprogramming of cells in the tumor microenvironment, or (iii) modification of the extracellular microenvironment [46], [34], [47].

2. AIM OF THE WORK

The aim of this work was investigate the implication of V-ATPase proton pump in human glioma and in contributing to the maintenance of the glioma stem cell niche. In this context, we aimed to understand the role of V-ATPase in the modulation of glioma stem cells EVs signaling.

3. MATERIAL AND METHODS

3.1 Generation of primary, patients derived, GBM cultures

Primary cells were isolated directly from patient's sample after surgery resection (enrolled at Fondazione IRCCS Ca' Granda Ospedale Maggiore Policlinico (Milan, Italy)). Samples obtained from tumor core (GBM cells, n= 51) and/or healthy tumor margins (MG tumor cells, n=20) were disaggregated enzymatically and mechanically using tumor dissociation kit (Miltenyi kit - 130-095-929). After that, cells were washed two times with HBSS (14175-053 Gibco) and seeded in Neurocult medium supplemented with growth factors (NC #05751, bFGF #78003, EGF #78006.1 – Voden) (undifferentiated condition) or RPMI (61870-010 Gibco) supplemented with 10% (vol/vol) FBS (10270-106 Gibco) (differentiated condition). MG tumor cells were maintained until one month in culture.

GBM tumor cells maintained in undifferentiated condition, whether are rich in stem cells, are naturally able to form neurospheres (NS) after 2-6 weeks in culture.

3.2 RNA extraction and qRT-PCR

Total RNA was purified from cell cultures using Master Pure RNA purification kit (Epicentre Biotechnologies, Illumina; Madison, WI, USA). Gene expression was then quantified by qPCR (using TaqMan assays) together with a reference gene (B2M and/or 18S RNA) or using *TaqMan® Array Human Molecular Mechanisms Of Cancer 96-well plate* (Life Technologies, MA, USA) (Table1).

Pathways		Investigated	Vehiculated
	V-ATPase subunits	17	14
	Cell cycle	5	5
Cancer pathways	MAPK/Erk pathway	7	7
	Akt pathway	4	1
	Other	3	2

Tab. 1_mRNA investigated in exosomes

miRNA from cells and RNA and miRNA from extracellular vesicles were extracted using miRVANA kit following manufacturer procedures. mRNA was pre-amplified using custom PreAmp primers and its expression is investigated using custom Applied Biosystems TaqMan Card. miRNAs were retrotranscribed using Megaplex RT primers (Human pools A and B v3.0) and Taqman MicroRNA Reverse Transcription kit, then pre-amplified using Megaplex PreAmp primer Human pools A and B. miRNA profiling was investigated using TaqMan™ Array Human MicroRNA A+B Cards Set v3.0 that allow to investigate the expression of 754 human miRNAs. All reagents, kits and instrumentation used were purchase from Life Technologies (Waltham, MA USA).

For co-culture study, mRNA was extracted after 24 hours and 3 days and miRNAs after 12 and 24 hours (GBM and MG tumor cells respectively) from exosomes addition to MG and GBM tumor cells. Whereas mRNA was extracted after 6 and 90 days from LO addition to recipient cells.

3.3 Antibody and reagents

Lysotracker, Cell Trace, FM lipophilic styryl dyes, sytoRNA and exosome spin columns were purchased from Life Technologies (L12492, C34557, F34653, S32703,-4484449 respectively). Annexin V was obtained from BD (556419), Bafilomycin A1 (sc-201550) and Concanamycin A (sc-202111) from Santa Cruz. qEV columns were purchased from Izon and stored in

PBS at 4°C. Optiprep was purchased from Sigma-Aldrich. The following antibodies were used for immunofluorescence, western blot and flow cytometry: ATP6V1G1 (Proteintech, 16143-1-AP), ATP6V0C (Novusbio, NBP1-31492), ATP6V0A2 (SIGMA, SAB2100187), ATP6V1C1 (Sigma-Aldrich, HPA023943), Vinculin (SIGMA, V9131), p44/42 MAPK (Cell Signaling, #4695), Phospho-p44/42 MAPK (Cell Signaling, #8544), phospho-mTOR (Cell Signaling, #2475), mTOR (Cell Signaling, #2983), pan-Akt (Cell Signaling, #4691), phospho-Akt (Cell Signaling, #4060), Tsg101 (Proteintech, 14497-1-AP), Ago2 (Proteintech, 10686-1-AP), Clathrin (abcam, ab23440), CD63 (Santa Cruz, sc-15363), CD9 (WB: Thermo Fisher, 10626D – FACS: Miltenyi, 130-103-988), CD81 (Miltenyi, 130-107-982), Calnexin (abcam, ab31290), Nestin (R&D, MAB 1259), Tuji (SIGMA, T3952), GFAP (SIGMA, G9269), CD11b (Proteintech, 20991-1-AP), O4 (SIGMA, O7139), Olig2 (SIGMA, AV32753), CD31 (abcam, ab28364), Vimentin (Miltenyi, 130-106-369), Ki67 (abcam, ab15580).

3.4 Evaluation of V-ATPase impairment effect

To evaluate cell growth rate, NS were followed for 10 days (snapped every 24 hours) using a time-lapse microscope (Eclipse Ti-E, Nikon Instruments, Florence, Italy), the diameter of NS was evaluated using ImageJ software (manual quantification) and for each experiment was calculated the mean diameter of 10 different NS. To evaluate spheres-forming ability after V-ATPase inhibition, NS were resuspended at single cell, treated with Bafilomycin A1 at time zero and followed for 72 hours. The number of spheres were manually counted for each time points. Both experiments were repeated three times.

To evaluate cell invasion, NS were embedded in type I collagen (SIGMA, c4243) and allowed to move for 48 hours, in presence or absence of

Bafilomycin A1. Also in this case, cultures were followed using the time-lapse microscope. Images for each sample were snapped every 2 hours and then assembled into a movie in QuickTime format. The radius of invasion was evaluated using Volocity software (Volocity 6.3, Perkin Elmer), for each spheres were calculated the mean of 10 different invading cells.

For cell death (Annexin V) and lysosomal acidification (Lysotracker) NS and/or Diff cells were seeded, and after 24 hours treated with Bafilomycin A1 or Concanamycin A or vehicle. Two days after treatment, the two assays were performed adding the respective probe to the cultures. Fluorescence was captured using time laps microscope and the quantification was calculated after setting the threshold on unlabeled samples, and the mean intensity of the fluorochrome was calculated using ImageJ software.

3.5 Immunofluorescence analysis

For immunofluorescence experiments, monolayer cultures were grown on cover-glasses whereas NS were cyto-spinned on charged slides for 3 minutes at 900rpm (Thermo Scientific, Waltham, MA, USA). Cells were first fixed in PFA 4% for 15 (monolayer cultures) or 30 minutes (NS), quenched for green auto-fluorescence using glycine 20mM for 20 minutes and then permalized with Triton 0.5% for 30 minutes at room temperature. Cells were saturated with BSA 10% for 1 hour at room temperature. Primary antibodies, diluited 1:100 in PBS-BSA 10%, were incubated overnight at 4°C and fluorescence conjugated secondary antibody (1:1000) 1 hour at room temperature, finally cells were stained with Hoechst for 5 minutes at room temperature and mounted (table 2). Confocal images were generated with a Leica TCS SP5 Confocal microscope with a magnification of 40X, z-

stack images were captured every 0,46µm (Leica Microsystems). Fluorescence quantification was calculated on full cell stacks after setting the threshold on unlabeled samples, and the mean intensity of the fluorochrome was calculated using ImageJ software. The number of positive nuclei was calculated using Volocity software (find object plugins) and normalized on total number of nuclei.

Primary Ab			Secondary Ab			Confocal setting	
Name	Species	Dilution	Dilution	Excitation (nm)	Emission (nm)	Objective	Pinhole
Nestin	Mouse	1:100	1:1000	568	580-620	63X	1 AU
Sox2	Rabbit	1:100	1:1000	488	510-540	63X	1 AU
Olig2	Mouse	1:100	1:1000	568	580-620	63X	1 AU
Tuji	Rabbit	1:100	1:1000	488	510-540	63X	1 AU
Gfap	Rabbit	1:100	1:1000	488	510-540	63X	1 AU
O4	Mouse	1:100	1:1000	568	580-620	63X	1 AU
V1G1	Rabbit	1:100	1:1000	568	580-620	40X	1 AU
V1C1	Rabbit	1:100	1:1000	488	510-540	40X	1 AU
V0A2	Rabbit	1:200	1:1000	488	510-540	40X	1 AU
V0C	Rabbit	1:100	1:1000	488	510-540	40X	1 AU
Ki67	Mouse	1:200	1:1000	488	510-540	40X	1 AU
pERK 1/2	Rabbit	1:100	1:1000	568	580-620	40X	1 AU

Table 2_Immunofluorescence antibodies.

3.6 Cancer 10-pathway Reporter Arrays

The Cancer 10-pathway Reporter Luciferase Kit (CCA-001L, Tube Format, Qiagen) is a commercial reporter array that allows measurement of ten cancer-related signaling pathways. Each tube contain a mixture of an inducible transcription factor responsive firefly luciferase reporter and constitutively expressing Renilla construct (40:1). Tecan Infinite F200 was used for signal detection. Investigated cancer pathway were: Wnt (TCF/LEF), Notch (RBP-Jκ), p53/DNA Damage (p53), TGFβ (SMAD2/3/4), Cell cycle/pRb-E2F (E2F/DP1), NFκB (NFκB), Myc/Max (Myc/Max), Hypoxia (HIF1A), MAPK/ERK (Elk-1/SRF) and MAPK/JNK (AP-1). NS were transfected with Lipofectamine 3000 (L3000015, Invitrogen) following

manufacture datasheet. Firefly luciferase and Renilla were measured after 48h from transfection (in each experimente were valuated the mean of experimental duplicate), experiment was performed two times on 6 different NS (3 $V1G1^{LOW}$ and 3 $V1G1^{HIGH}$).

3.7 Extracellular vesicles production from NS

3.7.1 Electron microscopy

For electron microscopy analysis NS, with or without Bafilomycin A1 treatment, were fixed in 2.5% glutaraldehyde in 100 mM phosphate buffer at pH 7.0 for 1 hour at room temperature (to preserve the structure of the cells with the minimum of alteration from the living state). Then cells were processed and included in resin embedding according to [48] by Electron Microscopy Unit at San Paolo Hospital (thanks to Paola Braidotti).

Images were captured using electron microscope of Alembic San Raffaele Unit (thanks to Maria Carla Panzeri). In order to investigate the presence of multivesicolar bodies, intracellular images were captured at 1840X magnification, whereas to study the presence and production of extracellular vesicles (exosomes, ectosomes and large oncosomes) extracellular mileu images were captured at 5000X magnification.

3.7.2 Confocal images

To investigate EVs production in live NS, cells were incubated for 30 minutes at 37°C with FM 1-43 FX at 40uM and wash two times in PBS. NS were seeded on glass bottom well (MatTek) and followed with live confocal microscope for 20 minutes in gas/humidification chamber (images of full NS were captured every 5 minutes). Large oncosomes are clearly visible as evagination of plasma membrane (dimension between 1 and 5um).

To investigate V1G1 presence on large oncosomes membrane, NS were seeded on poly-L-lysine (SIGMA, P8920) coated slices (slices were coated

for 20 minutes at 37°C) for 1 hours at 37°C. Then NS were labeled with FM 4-64 FX for 30 minutes at 37°C, washed with PBS and fixed 10 minutes with PFA 2%. Primary (1:100) and secondary (1:1000, alexa-fluor 488) antibody were incubated 1 hours and 30 minutes respectively, both at room temperature. Z-stack images were captured using confocal microscope (63X magnification) and single stack images were captured with optical zoom of 5X.

3.8 Isolation of extracellular vesicles and characterization

3.8.1 Isolation

Extracellular vesicles were isolated from supernatant of neurospheres (n=12) at basal condition after 48 hours from change medium and after 24 hours from 5nM Bafilomycin A1 treatment. Cells were pelleted at 250rcf for 5 minutes and supernatant were collected and concentrated using Amicon Ultra centrifugal filter tubes (Millipore) (stored at -80°C). Then collected supernatant were centrifuged at 1000rcf for 10 minutes at 4°C to remove debris and/or apoptotic bodies (pellet). From supernatant large oncosomes (LO) were isolated through centrifugation at 10.000 rcf for 30 minutes at 4°C and maintained at -80°C (pellet was re-suspended in 0,2µm filtered). Exosomes were isolated from supermatant by qEV size exclusion column (SEC – iZON) as described in Lobb et al. [49]. Briefly, 500ul of concentrated supernatant (depleted of debris and LO) was overlaid on qEV column followed by elution with PBS, 500ul phases were collected in eppendorf, exosomes are present in phases 6-7-8. [50], [51]

3.8.2 Electron microscopy and immuno-gold staining

Quality and purity of exosomes and LO were evaluated through electron microscopy, following the protocol present in Lobb et al. [49].

In order to evaluate the presence of V1G1 subunits on exosomes and LO surface, an immune-gold staining was carried out using ATP6V1G1 antibody (Proteintech, Manchester, United Kindom).
Both analysis were performed with the support of Alembic San Raffaele Unit (thanks to Maria Carla Panzeri). Images were captured at 12500 and 20000X magnification.

3.8.3 Nanoparticle tracking analysis (NTA)

The concentration and size distribution of particles were analyzed with Nanosight NS300 (Malvern, Instruments Ltd Worcestershire, UK) with the support of Valentina Bollati laboratory (Dipartimento di Scienze Cliniche e di Comunità, Università degli Studi di Milano).

3.8.4 EVs internalization

For internalization study, vesicles were stained with PHK26 (SIGMA, MINI26). In particular, medium collected from NS culture in different conditions, after debris elimination, was ultra-centrifugated at 100.000 rcf at 4°C (rotor SW 41Ti) for 2 hours. PHK26 was added to pellet for 5 minutes at room temperature; staining was blocked adding 10% BSA (SIGMA) in PBS. LO were pelleted at 10.000rcf for 30 minutes and washed 3 times. In order to eliminate not bind PHK26 from exosomes preparation, they were isolated using an optiprep density gradient [49]; briefly, a discontinuos iodixanol gradient was prepared by diluting optiprep (60%w/v) with 0.25M sucrose, 1mM EDTA and 10mM Tris-HCL (pH 7.4) to generate 40%, 20%, 10% and 5% w/v. With care, gradient was generated by sequentially layering 3ml of 40, 20, 10 and 5% on exosomes pellet, in ultraclear Beckman Culture centrifuge tubes. Gradient was centrifugated for 18 hours at 100.000 rcf with a SW 41Ti rotor. 1ml fraction was collected from the top, fraction 6 and 7 (contained exosomes) were diluted to 20ml in PBS and centrifuged at 100.000rcf for 2 hours at 4°C with a Type 50.2 Ti rotor. The

resulting pellets were resuspended in PBS (10ul for 1ml of medium) and conserved at -80°C.

Recipient cells (GBM or MG tumor cells) were seeded on 96 glass bottom multiwell plates at 80% of confluence (MatTek Ashland, MA) and stained with cell trace (5µm, cytoplasm staining) and cells mask (1:1000, cytoplasm and plasma membrane staining) for 30 minutes at 37°C in PBS, in both case cells were washed two times with PBS and fresh medium was added. After 24 hours the equivalent of 250ul of supernatant of EVs was added to cells. LO internalization was evaluated after 6 and 24 hours of co-culture in live cells using live confocal microscopy (37°C in humidification chamber) with a 63X objective. Leica software tools *line profile – intensity – sort ROI* (Leica Microsystems LAS AF 2.6.0.7266) was used to discriminate LO internalized in recipient cells from LO bind to plasma membrane. In particular for each image was investigated the intensity of different line profiles (ROI in figure 8) in 3 z-stack (two ends and center of recipient cells) and based on picks' profile is possible study LO internalization (Figure 8).

Whereas, exosomes internalization was followed using flow citometry after 2, 6 and 24 hours.

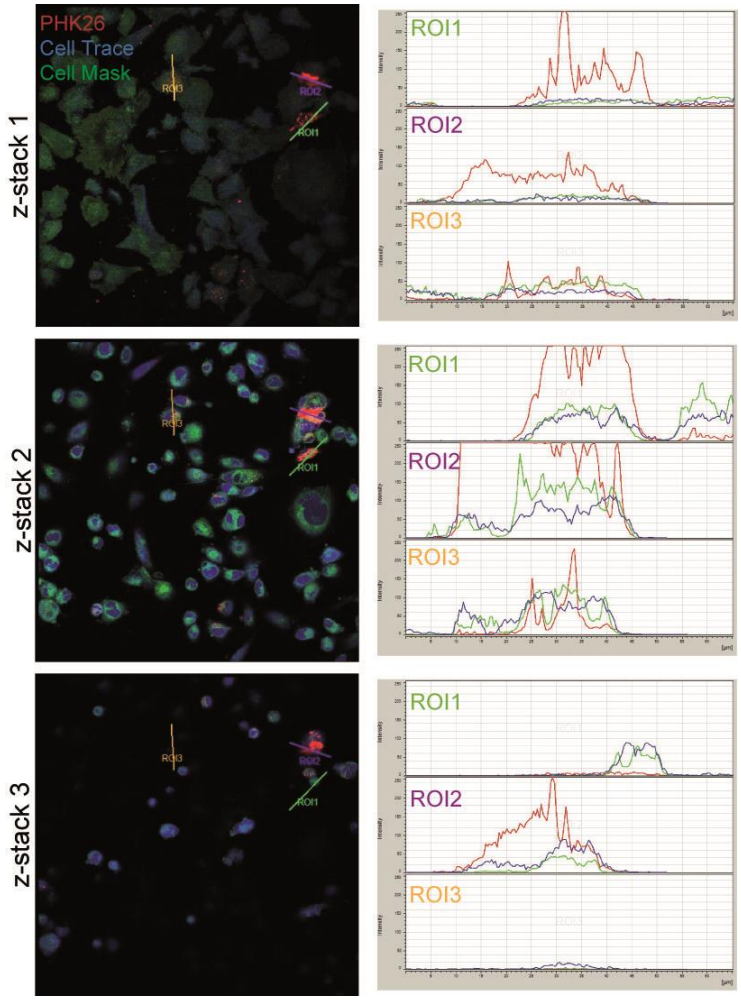

Figure 8_Rapresentative images of LO internalization study using Leica software. ROI1 and ROI3 represent LO internalized in recipient cells, in fact red (PHK26) pick appear always with and within the blue and green picks (cell trace and cell mask). Instead ROI2 shows LO bind to plasma membrane of recipient cells and not yet internalized, in fact both in stack-1 and in stack-3 red pick appear without green and blue picks.

3.9 Western blot analysis

Total cells and isolated EVs were lysed in buffer composed by Tris-HCl (50mM), NaCl (137mM), 1% Triton X-100, 0,1% SDS, phosphatase inhibitor and protease inhibitor (pH 7.6-8); for EVs isolation 3% SDS was

added previously of use. After lysis EVs and cells were sonicated 5 times (30'' ON/ 30'' OFF), pelleted at 15.000rcf to eliminate debris and quantified using microBCA (Thermo Fisher Scientific, Waltham, MA USA).

Protein (40µg) were boiled for 5 minutes at 95° (not reducing condition for CD63 staining), resolved by SDS-PAGE, transferred to nitrocellulose membrane, blocked in 5% not-fat powdered milk in PBS-T (1% Tween-20) and probed with antibodies (table 3).

In MG tumor cells co-cultured for 3 days with exosomes PathScan Intracellular Signaling Membrane Array Kit (Cell Signaling) was used to simultaneous detection of phosphorylation or cleavage of 18 signaling molecules involved in cancer pathway.

Primary Ab				Secondary Ab		
Name	Species	Dilution	Buffer	Dilution	Type	Buffer
V1G1	Rabbit	1:1000	5% BSA-PBS-T	1:5000	HRP	5% Milk-PBS-T
V1C1	Rabbit	1:500	5% BSA-PBS-T	1:5000	HRP	5% Milk-PBS-T
V0A2	Rabbit	1:1000	5% BSA-PBS-T	1:5000	HRP	5% Milk-PBS-T
V0C	Rabbit	1:500	5% BSA-PBS-T	1:5000	HRP	5% Milk-PBS-T
ERK 1/2	Rabbit	1:1000	5% BSA-PBS-T	1:5000	HRP	5% Milk-PBS-T
pERK 1/2	Rabbit	1:1000	5% BSA-PBS-T	1:5000	HRP	5% Milk-PBS-T
AKT	Rabbit	1:1000	5% BSA-PBS-T	1:5000	HRP	5% Milk-PBS-T
pAKT s473	Rabbit	1:500	5% BSA-PBS-T	1:5000	HRP	5% Milk-PBS-T
mTOR	Rabbit	1:1000	5% BSA-PBS-T	1:5000	HRP	5% Milk-PBS-T
p-mTOR	Rabbit	1:1000	5% BSA-PBS-T	1:5000	HRP	5% Milk-PBS-T
CD9	Rabbit	1:500	5% Milk-PBS-T	1:5000	HRP	5% Milk-PBS-T
CD63	Rabbit	1:200	5% Milk-PBS-T	1:5000	HRP	5% Milk-PBS-T
Tsg101	Rabbit	1:1000	5% BSA-PBS-T	1:5000	HRP	5% Milk-PBS-T
Clathrin	Rabbit	1:1000	5% Milk-PBS-T	1:5000	HRP	5% Milk-PBS-T
Calnexin	Rabbit	1:1000	5% Milk-PBS-T	1:5000	HRP	5% Milk-PBS-T
Ago2	Rabbit	1:400	5% BSA-PBS-T	1:5000	HRP	5% Milk-PBS-T
Vinculin	Mouse	1:1000	5% Milk-PBS-T	1:5000	HRP	5% Milk-PBS-T

Table 3_Western blot antibodies.

3.10 Flow cytometry

For characterization study, cells were fixed in PFA 2% for 10 minutes, permeabilized in Triton 0.1% for 10 minutes and stained with primary (1:100 - 1 hour) and secondary antibody (1:1000 - 30 minutes) at room

temperature. Non marked cells were used as negative control, whereas cells incubated with normal immunoglobulin of the same isotype of primary antibody were used as isotype control.

For exosomes staining and characterization, after staining they were bind to CD63-coated beads (Thermo Fisher, 10606D) in order to avoid dimension limit. In particular exosomes were stained with CD9 and CD81 or with V1G1 primary antibody for 1 hour at room temperature (1:1000), and (only for V1G1 antibody) 30 minutes with secondary antibody (1:1000) and 20 minutes at 37°C with Cell Trace (5µm) and SytoRNA (10µm). According to manufacture protocol, exosome spin columns were used in order to remove not incorporated dye from exosomes preparation. Then exosomes were bound to beads in wheel overnight at 4°C. Exosomes isolated from NC free medium was used as negative control. [52]

FACS Canto I and FlowJo V.10.1 software were used for analyses.

3.11 EVs biological effect

In order to investigate EVs biological effect, cell growth, cell cycle, proliferation, cell motility and spheres formation were evaluated. In particular recipient cells (MG and GBM tumor cells) were seeded on 48 (spheres formation), 24 (cell growth and cell motility) or 6 multiwell (cell cycle) after patient's sample disaggregation. After a variable period of 6-10 days (when cells seeded are at a 60% of confluence) the equivalent of 500µl (40 well), 1ml (24 well) or 3ml (6 well) of supernatant of EVs was added. For cell growth, cells were stained with cell trace (5µm for 20 minutes at 37°C) and cell divisions were valuated as reduction intensity (caused by redistribution of probe in daughter cells) using flow cytometry; GBM tumor cells were followed for 24 hours, instead MG cells until 17 days. Cell cycle was investigated as DNA content by propidium iodide

staining, in particular cells were fixed with cold absolute EtOH after 24 hours (GBM cells) or 3 days (MG cells) in ice overnight, then cells were washed two times with PBS-1% FBS and stained with 500µl of PI/RNase Staining Buffer (550825 BD, PI is detected in the orange range of the spectrum using a 562-588 nm band pass filter). FACS Canto I and FlowJo V.10.1 software were used for analyses.

Proliferation was evaluated as nuclear staining for Ki67 (table 2) after 24 hours (GBM cells) and 3 days (MG cells) of co-culture. Confocal images were generated with a Leica TCS SP5 Confocal microscope (40X magnification).

To evaluate cell motility, GBM tumor cells were seeded and conditioned for 24 hours with exosomes, then a gap was created with a 200µl tip and cells were followed for 65 hours, every 4 hours, using Nikon time laps microscope. In particular cells were maintained in gas/humidification controlled chamber at 37°C and images were captured in bright field with 10X objective. Migration was manually measured as distance between the edges of the wounds (in 6 different points for wounds) and then normalized on gap dimension at time zero, using ImageJ software.

For spheres formation study, the equivalent of 1ml of supernatant of EVs was added to GBM tumor cells maintained in undifferentiated condition and spheres formed were counted at 3 and 6 days. After 6 days from starting of co-culture, formed spheres were picked and seed in a different plate (whereas, RNA from GBM cells adherent was extracted). Medium was changed once a week and spheres were followed until 90 days from starting of co-culture.

3.12 Statistical analyses

Statistical analysis was performed using GraphPad Prism software (La Jolla, CA, USA) and environment R (R Development Core Team, 2005). All GraphPad Prism graph show mean with standard deviation (SD). Additional software packages (ComplexHeatmap, samr) were taken from the Bioconductor project. SAM analysis were performed to identify miRNAs classes associated, (q.value <0.05, FC> 1 abs).

All biological experiment was performed at least three times (all single experiment has an technical duplicate). In particular NS experiments (gene and protein expression at basal level and after differentiation or treatment, lysotracker, cell death, cell growth, cell invasion and spheres formation) were performed on NS derived from 10 different GBM patient sample (5 $V1G1^{HIGH}$ and 5 $V1G1^{LOW}$) in triplicate. Exosomes and LO were isolated from 12 NS (half $V1G1^{HIGH}$ and $V1G1^{LOW}$) and data are a mean of experiment performed with EVs derived from all different patients. For GBM tumor cells as recipient cells, biological triplicate for each patients' sample were performed, instead for MG tumor cells (that doesn't survive for long period of time in culture) single biological replicate was performed, but it is increased number of patients' sample. In particular in this thesis were used GBM tumor cells derived from 10 different patients and MG tumor cells derived from 20 patients' sample. All experiment were repeated at least 4 times per condition.

To compare mean for two groups t-test was performed (Mann Whitney t-test), instead to compare three or more groups was used One-way Anova test (with Bonferroni post-test) and to determine how a response is affected by two factors was used Two-way Anova test (with Bonferroni post-test).

MicroRNA's targets identification were developed combined the results of MultimiR R package. The multiMiR database contains human data from

three validated miRNA–target databases (miRecords[D], miRTarBase[E] and TarBase[F]). Requiring the agreement of at least two of them to include a putative target in our analysis.

4. RESULTS

4.1 V-ATPase subunits expression in primary GBM cells

V-ATPase subunits expression was investigated in neurospheres (NS) and differentiated cells (Diff) (Figure 9) derived from 33 GBM patients (table 4). In particular, nine out of thirteen subunits of V1 sector (ATP6V1A, V1B, V1C1, V1C2, V1D, V1F, V1G1, V1G2, V1G3) and eight out of nine subunits of the V0 sector (ATP6V0A1, V0A2, V0A4, V0B, V0C, V0D, V0E, V0E1) were examined. ATP6V1F and ATP6V1G1 are the most expressed subunits both in NS and in Diff, whereas ATP6V1C2 and ATP6V0A4 are the least expressed ones (Fig. 10A). ATP6V1G1 resulted to be the most expressed subunit in NS, correlated to worse GBM patients' prognosis (Di Cristofori et al., Oncotarget 2015) and its levels decreased after NS differentiation. Therefore next analyses were focused on that subunit.

Interestingly, upon differentiation of NS into differentiated lineages (Fig. 9) ATP6V1G1 subunit was significantly down regulated both at gene (Fig. 10B) and protein (Fig. 10C-D) expression levels. After differentiation other V-ATPase subunits were down-regulated at gene levels, in particular ATP6V0A1, ATP6V1H and ATP6V0E (Fig. 10A), whereas ATP6V0D and ATP6V1G2 transcripts were up regulated in differentiated cells (Fig. 10B).

N°	SURGERY	SEX	Age (years)	DIAGNOSIS	GRADE	KI67	MGMT
28	27/05/2014	F	63	GBM	IV	35%	9%
30	30/06/2014	M	42	GBM	IV	>60%	2%
32	08/04/2014	F	78	GBM	IV	30-35%	62%
35	26/06/2014	M	29	GBM	IV	40%	6%
27	23/05/2014	F	82	GBM	IV	15%	4%
51	22/10/2014	M	59	GBM	IV	25-30%	4%
52	13/06/2014	M	53	GBM	IV	15%	3%
53	28/04/2014	M	64	GBM	IV	50%	4%
59	03/11/2014	M	55	GBM	IV	25%	2%
63	19/12/2014	M	64	GBM	IV	30%	3%
71	13/02/2015	F	76	GBM	IV	30-40%	27%
80	16/04/2015	M	72	GBM	IV	20%	8%
81	17/04/2015	M	52	GBM	IV	50%	32%
83	23/04/2015	F	54	GBM	IV	20%	29%
84	27/04/2015	F	72	GBM	IV	40%	20%
85	04/05/2015	F	57	GBM	IV	80%	2%
88	09/06/2015	M	51	GBM	IV	80%	19%
91	24/06/2015	M	75	GBM	IV	40%	3%
92	26/06/2015	F	78	GBM	IV	50%	50%
97	26/08/2015	M	49	GBM	IV	70%	2%
101	08/09/2015	M	80	GBM	IV	20-25%	2%
103	23/09/2015	M	64	GBM	IV	15%	3%
110	23/10/2015	M	47	GBM	IV	25-30%	63%
114	05/11/2015	M	60	GBM	IV	40%	3%
121	29/12/2015	M	69	GBM	IV	35%	21%
130	05/02/2016	M	45	GBM	IV	50%	15%
143	18/04/2016	M	59	GBM	IV	30%	4%
145	29/04/2016	F	69	GBM	IV	30%	2%
147	12/05/2016	M	75	GBM	IV	65%	55%
148	25/05/2016	M	45	GBM	IV	8%	51%
149	30/05/2016	F	58	GBM	IV	30%	21%

Table 4_Patient database

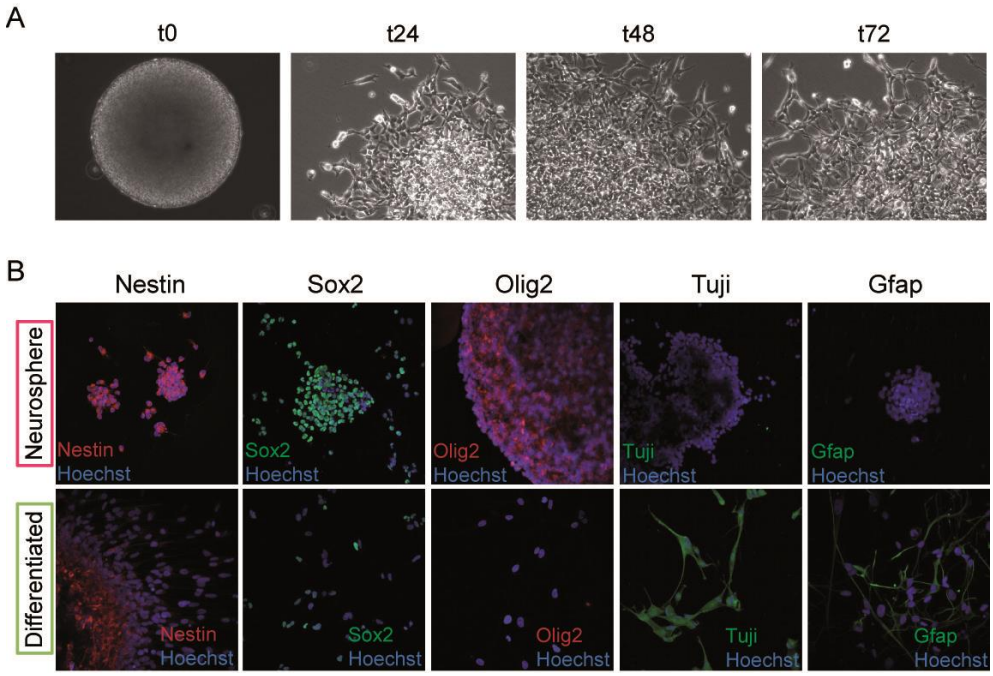

Figure 9_ Differentiation of GBM neurospheres in differentiated cells. Representative image of NS differentiation during time (captured with widefield microscope, 5X magnification - A). Protein expression in NS and Diff cells evaluated by immunofluorescence (captured with confocal microscope, 63X magnification, nuclear staining with Hoechst - B).

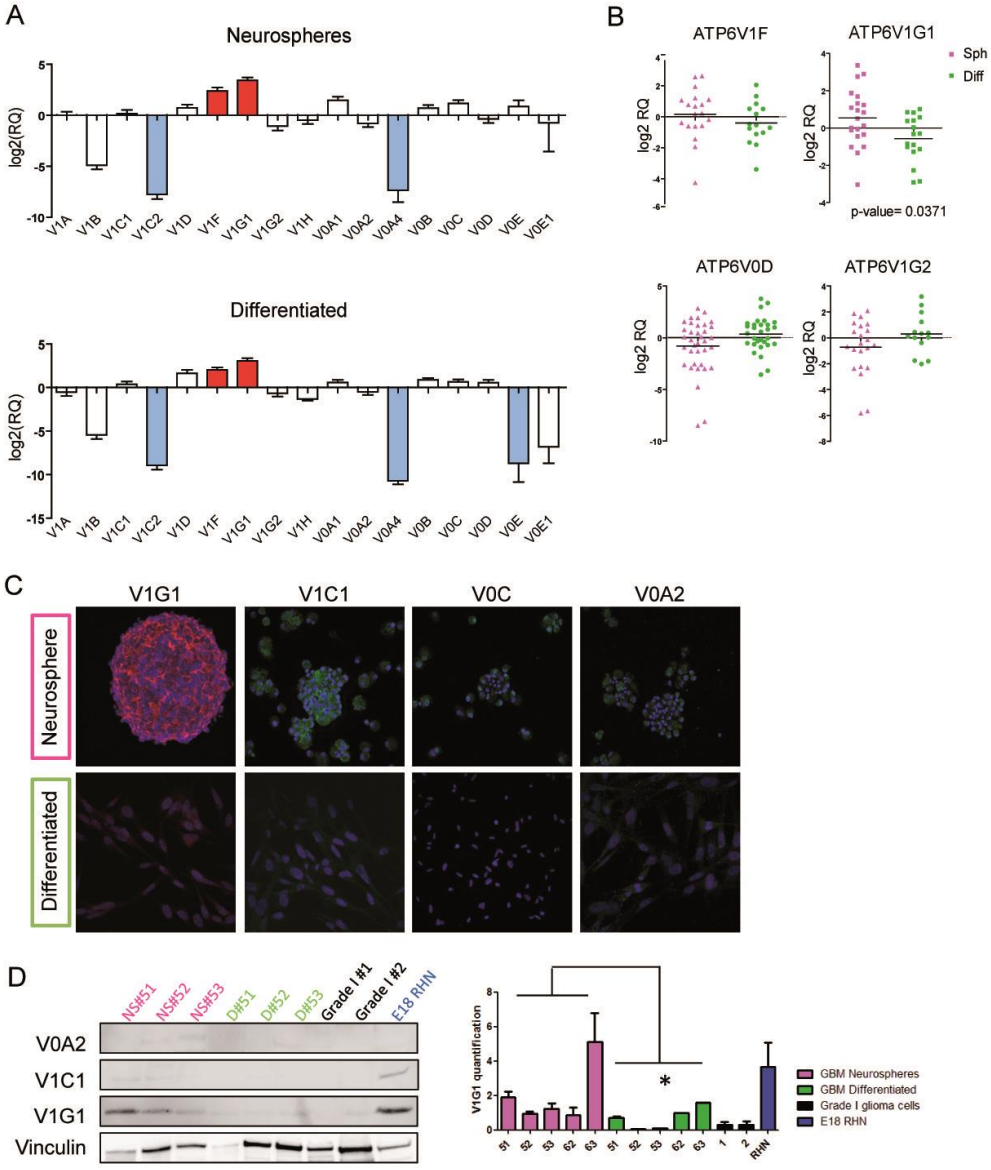

Fig.10_V-ATPase expression in primary GBM cells. V-ATPase subunits gene expression was investigated through TaqMan probe in quantitative real time PCR in NS and Diff cells derived from 33 GBM patients sample (A). Gene expression modulation after differentiation was investigated for 4 V-ATPase subunits (B). Protein expression in NS, Diff cells and patients samples was evaluated by western blot (D) and immunofluorescence (captured with confocal microscope, 63X magnification, nuclear staining with Hoechst - C). Vinculin, loading is used as control.

4.2 V-ATPase expression correlates with stemness features in GBM neurospheres

Since ATP6V1G1 expression decreased after differentiation, we decided to study the association between its expression and stemness features in NS. First, it was investigated gene expression of CD133, NESTIN, KLF4, NANOG, SOX2, OLIG2, POU3F2 and SALL2 in 21 NS samples. Unsupervised analysis revealed a correlation between ATP6V1G1 expression and stem genes (Fig. 11A). Moreover, primary cultures from tumors characterized by higher ATP6V1G1 levels formed spheres at higher rate than tumors with lower V1G1 expression (Fig. 11B). Accordingly we classified NS into $V1G1^{HIGH}$ (purple; n=10) and $V1G1^{LOW}$ (orange; n=11) and we analyzed their clonogenic and growth potentials.

$V1G1^{HIGH}$ NS grew more than $V1G1^{LOW}$ NS (Fig 11C-E) and formed a significantly higher number of spheres after desegregation (Fig 11D).

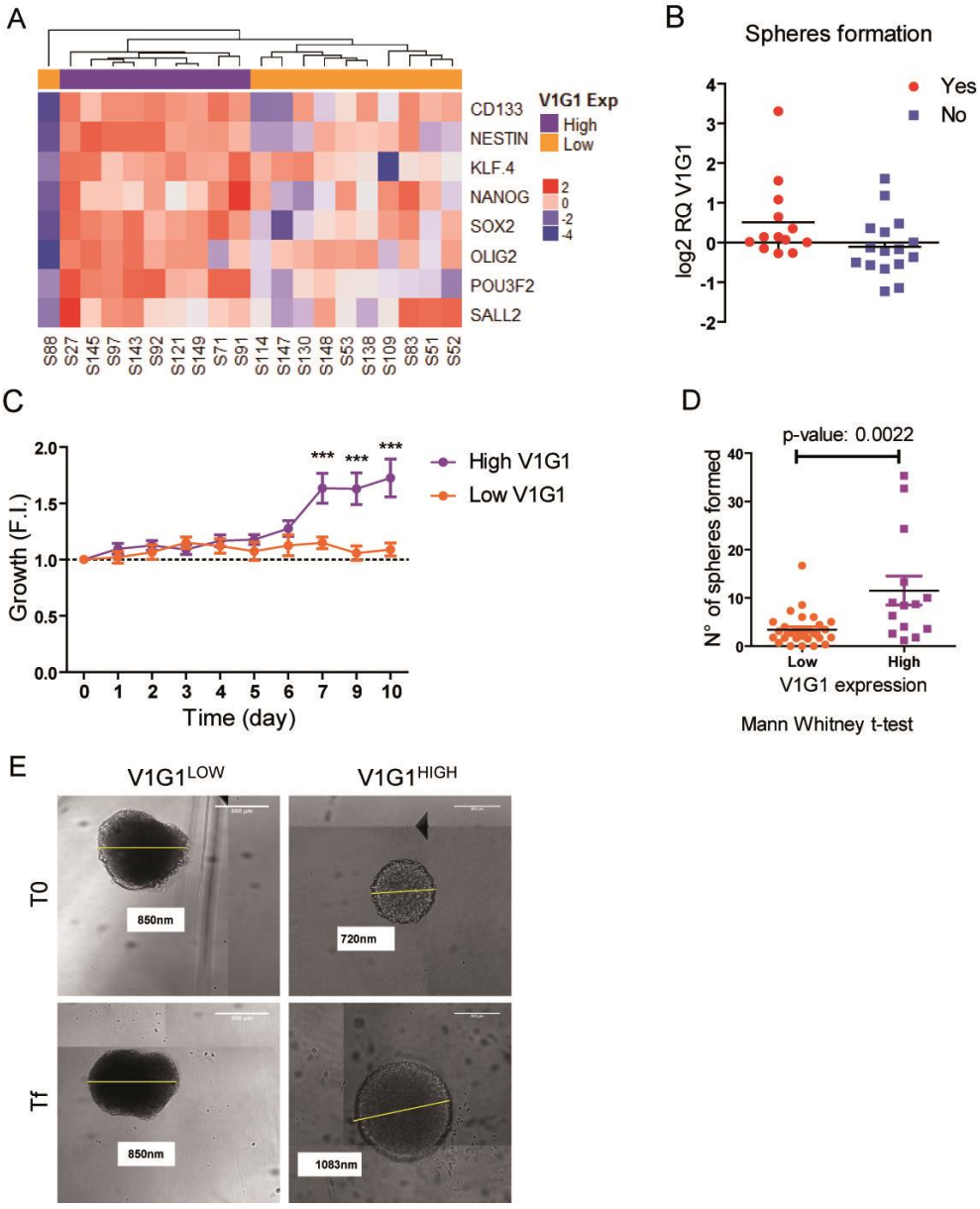

Fig.11_V-ATPase expression and clonogenicity. Heatmap shows the unsupervised analysis (average Euclidean metric) of stemness-related genes expression in NS (A). ATP6V1G1 gene expression in patients sample that are able or not to form NS (B). Growth index of NS, evaluated as diameter and number of NS, relative to T0 of NS (C-E, Two-way Anova, Bonferroni post-test as statistic). Number of spheres formed after desegregation, according to ATP6V1G1 expression (D, Mann Whitney t-test as statistic).

4.3 V-ATPase impairment through Bafilomycin A1 treatment

In order to investigate the role of V-ATPase proton pump in stem cells niche maintenance in human GBM, we treated NS with Bafilomycin A1 (BafA1), a drug able to block V-ATPase activity through binding to the V0 sector. To test the drug activity, we first evaluated the modulation of lysosomal acidification. Figure 12A shows that, at basal level, there are significant differences in lysotracker intensity between $V1G1^{HIGH}$ and $V1G1^{LOW}$ NS. Moreover, BafA1 treatment reduced lysosomal acidification both at 5nM and at 20nM dosages in NS (Fig. 12A), but induced cell death only at the dosage of 20nM (Fig. 12B). Conversely, in differentiated cells the proton pump impairment didn't induce cell death (Fig. 12D), despite lysosomal acidification was decreased (Fig. 12C).

Interestingly, BafA1 treatment at a non-lethal dosage (5nM) strongly reduced cell invasion of $V1G1^{HIGH}$ NS in a collagen matrix (Fig. 13A-B).

Finally, BafA1 treatment completely block the ability to reform spheres after disaggregation also at not lethal dosage (Fig 13C). This effect is related to a modulation of different stem genes, in particular NS BafA1 treatment at 5nM induce a significant reduction of POU3F2, SOX2 and NESTIN mRNA levels (Fig. 13D).

All these data support the hypothesis that the V-ATPase activity has a central role in GBM stem cells niche maintenance.

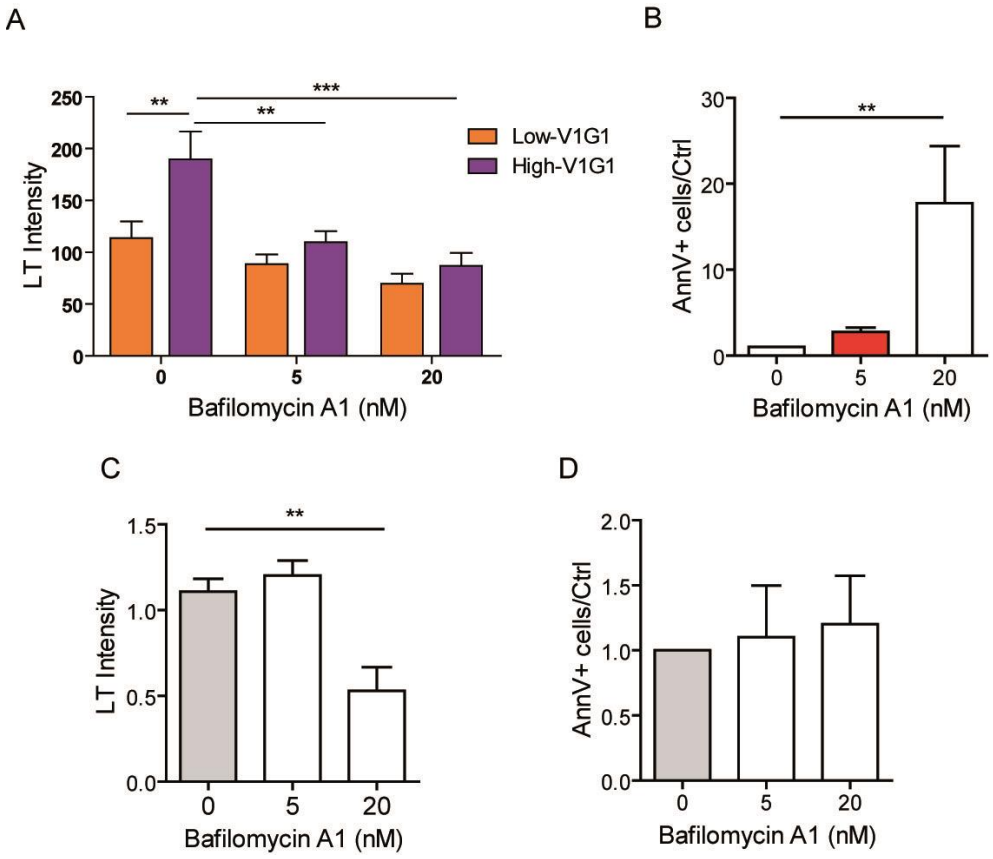

Fig.12_BafA1 treatment of GBM tumor cells. Lysosomal acidification was investigated using lysotracker probe (Life Technologies) in basal condition and after BafA1 treatment in NS (A) and differentiated cells (C) (Statistic: A One-way Anove, Bonferroni post-test; C Mann Whitney t-test, p=0.0078). The induction of cell death was analyzed through AnnexinV probe (BD) in NS (B; Statistic: Mann Whitney t-test, p=0.0010) and differentiated cells (D). All experiment was performed after 48hours of treatment, using Nikon time lapse microscopy. The ImageJ software was used for data analysis. For statistical analyses was performed non parametric t-test.

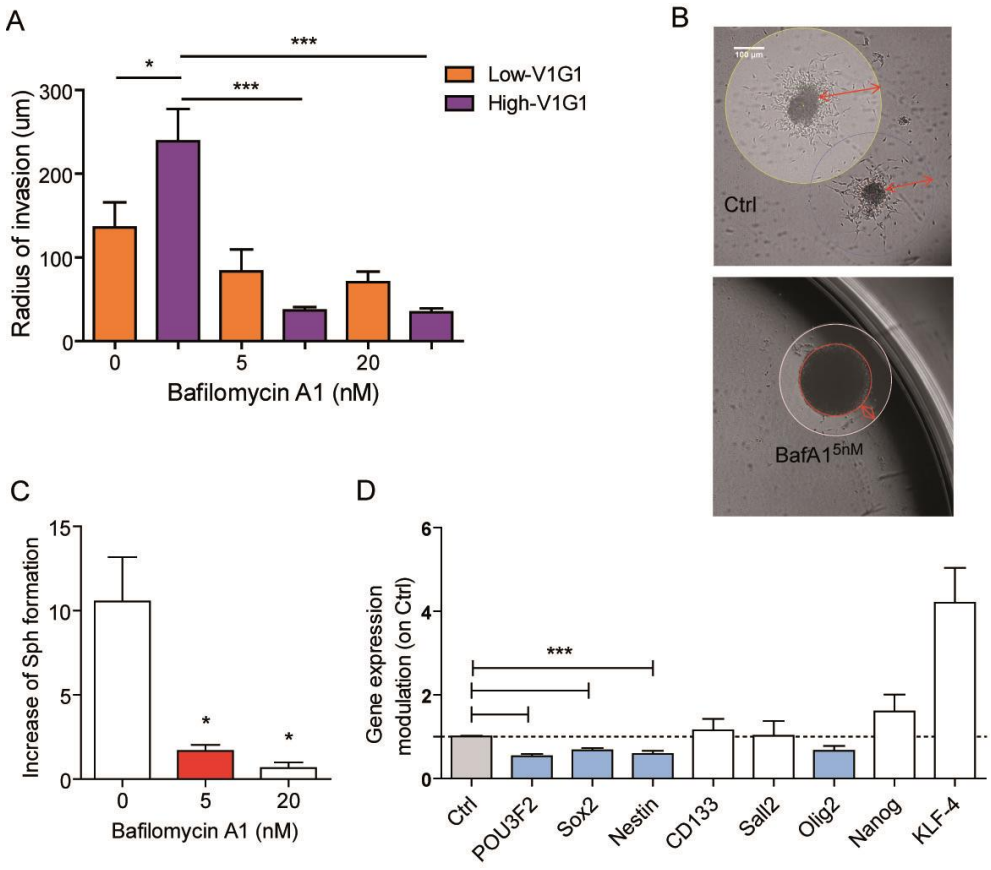

Fig.13_BafA1 treatment of GBM NS. Radius of invasion was studied in NS HighV1G1 and LowV1G1 after BafA1 treatment (A-B; Statistic: One-way Anove, Kruskall-Wallis test). Clonogenicity impairment after treatment was investigated as spheres formation (C; Statistic: Mann-Whitney t-test –p=0.0286) and stem genes modulation (D, Mann-Whitney t-test). All experiment was performed after 48hours of treatment, evaluated using Nikon time laps microscopy and quantified with ImageJ software.

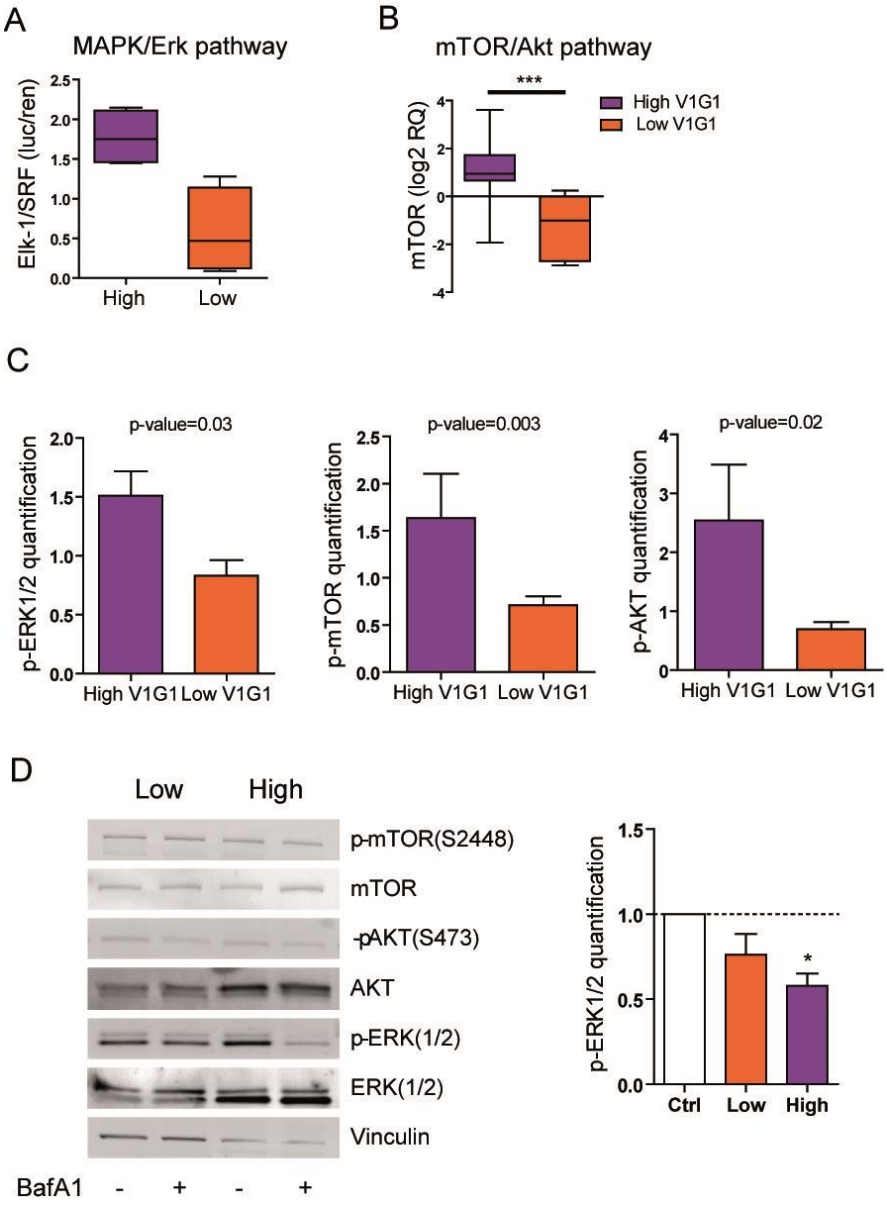

Fig.14_V-ATPase and MAPK pathway modulation. MAPK/Erk pathway activation at basal level was evaluated by synthesis of Elk-1/SRF transcription factor in HighV1G1 (n=3) and LowV1G1 (n=3) NS (A). mTOR gene expression was evaluated by quantitative Real Time PCR in HighV1G1 (n=6) and LowV1G1 (n=6) NS (B; Mann-Whitney t-test). Protein phosphorylation was investigated by western blot analysis and densitometry quantification was performed using ImageJ software, phosphorylated proteins were normalized on total proteins (basal level – C, after treatment – D). Vinculin is the loading control.

Then, the activation of cancer pathways in NS was screened using the Cignal Finder™ 10-Pathway Reporter Arrays. At basal levels, V1G1^{HIGH} NS showed higher activation of MAPK/Erk pathway (Fig. 14A) and, through quantitative real time PCR, mTOR gene expression (Fig. 14B). The differential activation of MAPK/Erk and mTOR/Akt pathway was confirmed at protein level by western blot analysis (Fig. 14C).
BafA1 treatment of V1G1^{HIGH}, but not V1G1^{LOW}, strongly reduces Erk1/2 phosphorylation, confirming its association with V-ATPase activity in NS (Fig. 14D).

4.4 GBM neurospheres produce different types of extracellular vesicles

Given the central roles of V-ATPase proton pump in regulating endosomal trafficking [30, 53, 54] and in glioma stem cells maintenance (Figs. 11-13), we investigated whether NS produce extracellular vesicles (EVs) and whether V-ATPase has a role on EV signaling in NS.
Electron microscopy (EM) analysis of NS showed different types of microvescicles were present in the extracellular space (Fig. 15). EM images demonstrate that NS produce both exosomes (Exo) (marked by nano-dimension, in green, and by the presence of multivescicolar bodies, in orange) and ectosomes (including large oncosomes (LO)) (micro-dimension, in purple, and originated directly by plasma membrane).

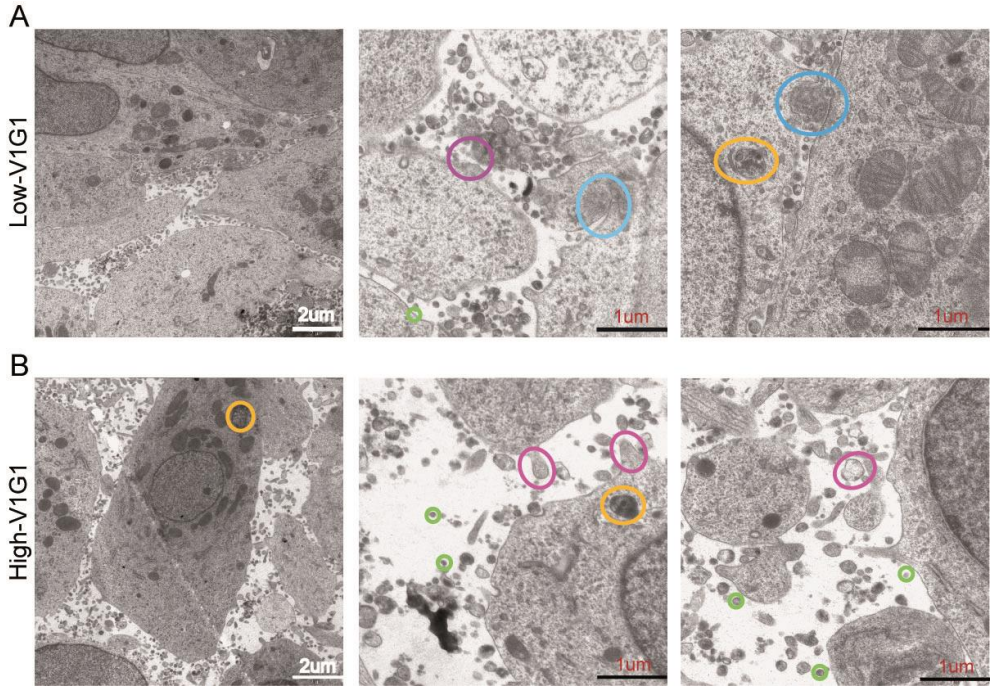

Fig.15_EVs production from primary GBM NS. EM images of NS producing Exo (green) and ectosomes (including large oncosomes); purple). Multivescicolar bodies are marked in orange when are inside the cells and in blue when they are fusing with the plasma membrane.

Exosomes and large oncosomes were then isolated from NS supernatant and characterized by EM, western blotting, Nanosight and FACS as raccomanded (Journal of Extracellular Vesicles in 2014 [55]). EM images show pure preparation of exosomes of the correct size (50-200nm) (Fig. 16A), and western blot analysis demonstrates the presence of exosome markers (CD9-CD63-Tsg101-Clathrin) and the absence of plasma cell marker (Calnexin) (Fig. 16B). Finally, exosomes bound to CD63-coated beads show the presence of CD9 and CD81 surface markers (Fig. 16C). In addition, exosomes had an integral membrane (as evidenced by cell trace staining; Fig. 16D) and contained ssRNA (as evidenced by sytoRNA staining; Fig. 16D).

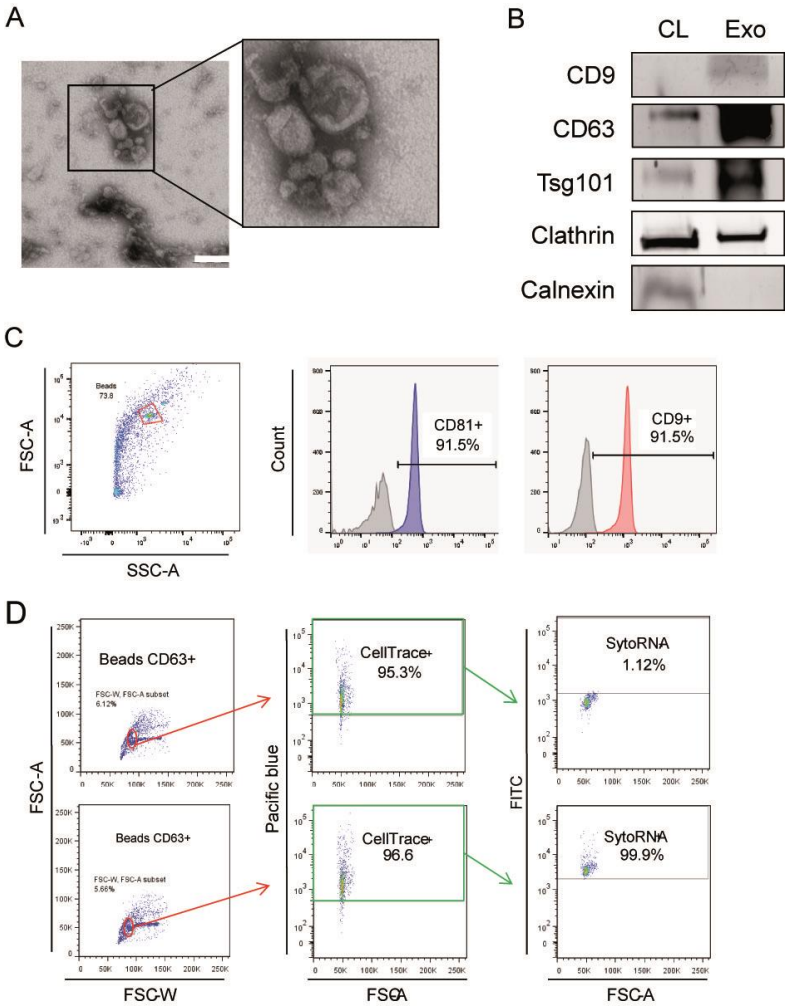

Fig.16_Exosomes characterization. EM image of exosomes (A), scale bar 200nm. Western blot analysis of cell lysate (CL) and exosomes (Exo) (B). FACS analysis of exosomes bind to CD63 beads (surface markers (C) and RNA (D)).

LO represent an additional class of tumor-derived EVs, so called because of an atypically large size and presence of abundant oncogenic cargos [35]. Thanks to their size (up to 10um), it is possible to follow their production and internalization using confocal microscopy. To this end, NS were incubated with FM 1-43 FX, wich, using ad hoc protocol, stains only plasma membrane vesicles. Through live confocal microscopy, NS producing LO

were followed every 5 minutes up to 20 minutes (Fig. 17A). Figure 17B showed LO generation from plasma membrane of NS. Through EM (17C) and IF (staining with PHK26) (17D) it was evaluated the quality of LO preparation (in both case is well visible the double-layers membrane and the absence of smaller vesicles). Then, the ssRNA content of LO was investigated through flow cytometry (SytoRNA dye; Fig. 17F). Western blot was performed to verify the presence of CD63 vesicles marker and the absence of exosomes (CD9) or cellular (calnexin) markers (Fig. 17E).

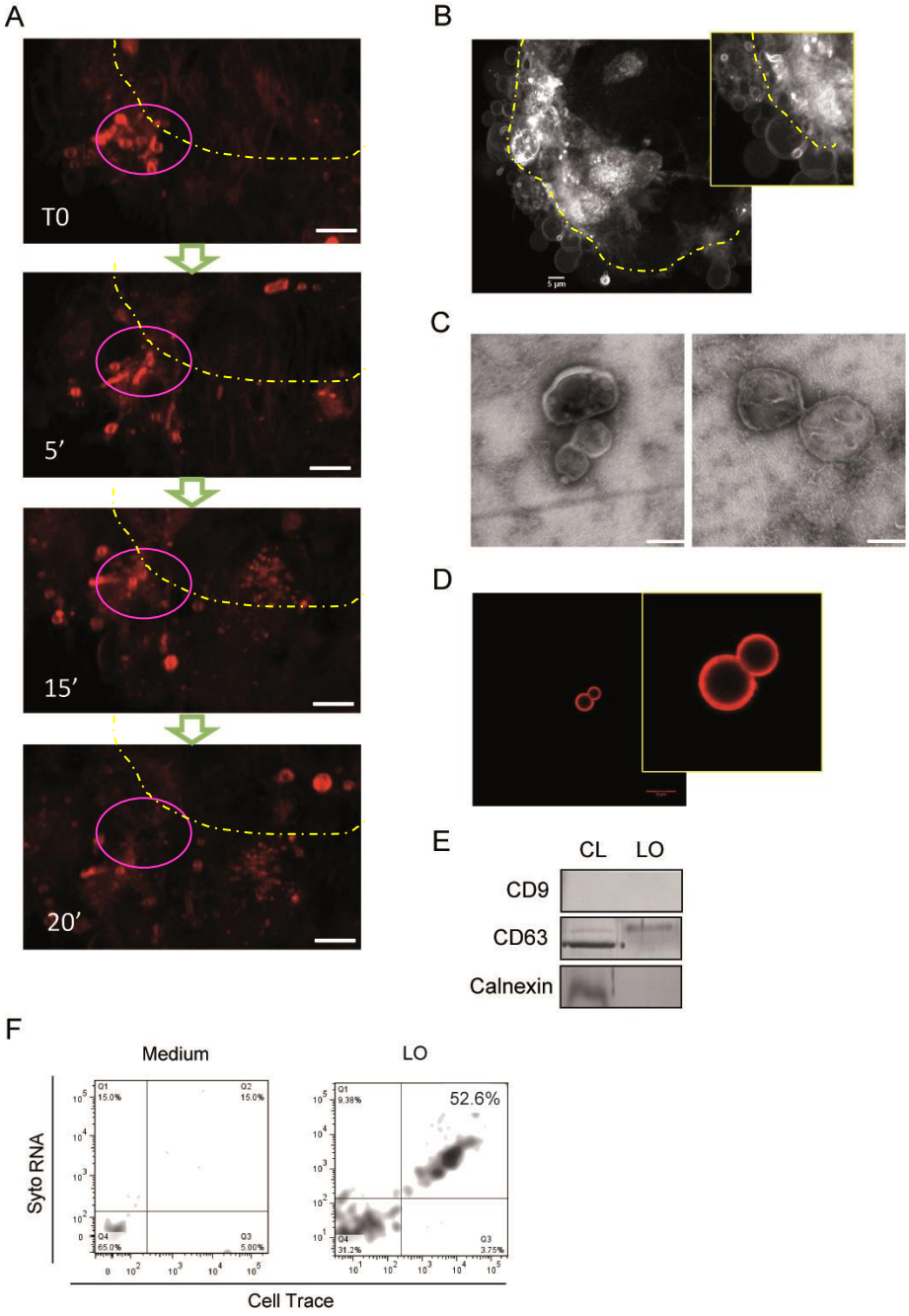

Fig.17_Large Oncosomes characterization. NS were stained with FM 1-43 FX and followed for 20 minutes using confocal microscopy (63X objective) (A). LO production was evaluated using confocal microscopy (63X objective and 3X zoom) (B). Electron microscopy image of LO (scale bar= 200nm) (C). Confocal image of

LO stained with PHK26 (scale bar= 10um) (D). FACS analysis of LO stained with cell trace (membrane integrity) and sytoRNA (ssRNA) (E). Protein content of cell lysate and LO (F).

4.5 EVs internalization in recipient cells

To gain functional cues into biological effects of exosomes and LO, we co-cultured different types of recipient cells with exo or LO purified from NS as described. Recipient cells were derived directly from patients sample. In particular, we prepared non-neoplastic cultures from tumor margins (MG) and tumor cultures from GBMs. All cell types were maintained both in differentiated (+FBS) or undifferentiated (-FBS) conditions. These cultures were characterized by immunofluorescence and cytofluorimetric analyses and the presence of heterogeneous cell populations (neurons, astrocytes, microglia and oligodendrocytes) could be determined in all cultures (Fig. 18A-B). Importantly, in both neoplastic and MG primary cultures no contaminant cells such as fibroblasts (Vimentin+) were present (Fig. 18A).

A

Cells Type	Ab	GBM (+FBS)	GBM (-FBS)	MG (+FBS)	MG (-FBS)
Neuron	Nestin	50.22%	60.9%	60%	46.1%
Neuron	Tuji	35.44%	60.6%	32.5%	57.5%
Astrocyte	GFAP	54.1%	34%	34%	53.6%
Microglia	CD11b	63.6%	65.7%	70.9%	55.9%
Oligodentrocite	O4	21%	33.9%	36%	41%
Oligodentrocite	Olig2	20%	38.6%	20.6%	30.3%
Endothelial	CD31	40%	54.6%	33.5%	26%
Fibroblast	Vimentin	0%	1%	0%	2%

B

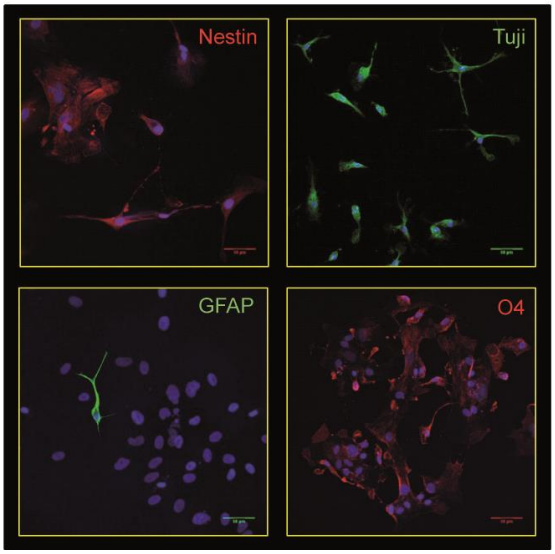

Fig.18_Primary cells characterization. Central nervous system cellular markers investigated through FACS on 3 different patients sample per condition (A). Representative image of immunofluorescence staining (B).

Extracellular vesicles derived from V1G1^{LOW} NS and V1G1^{HIGH} NS were stained with PHK26 probe (empty medium, NC, was used as control). LO were co-cultured with recipient cells for 6 and 24 hours. To test whether LO are internalized in recipient cells and not only bound to plasma membrane,

cells were stained with cell trace (staining of all cellular bodies) and cell mask (staining of cytoplasm and membrane) (Fig. 19B). Representative confocal image (Fig. 19A) captured after 24h of co-culture shows how LO^{HIGH} (LO derived from $V1G1^{HIGH}$ NS) have an higher ability to be internalized in recipient cells (Figs. 19A-C). The experiment was performed on different recipient cells in order to statistically count the percentage of PHK+ cells at different time point (Fig. 19C).

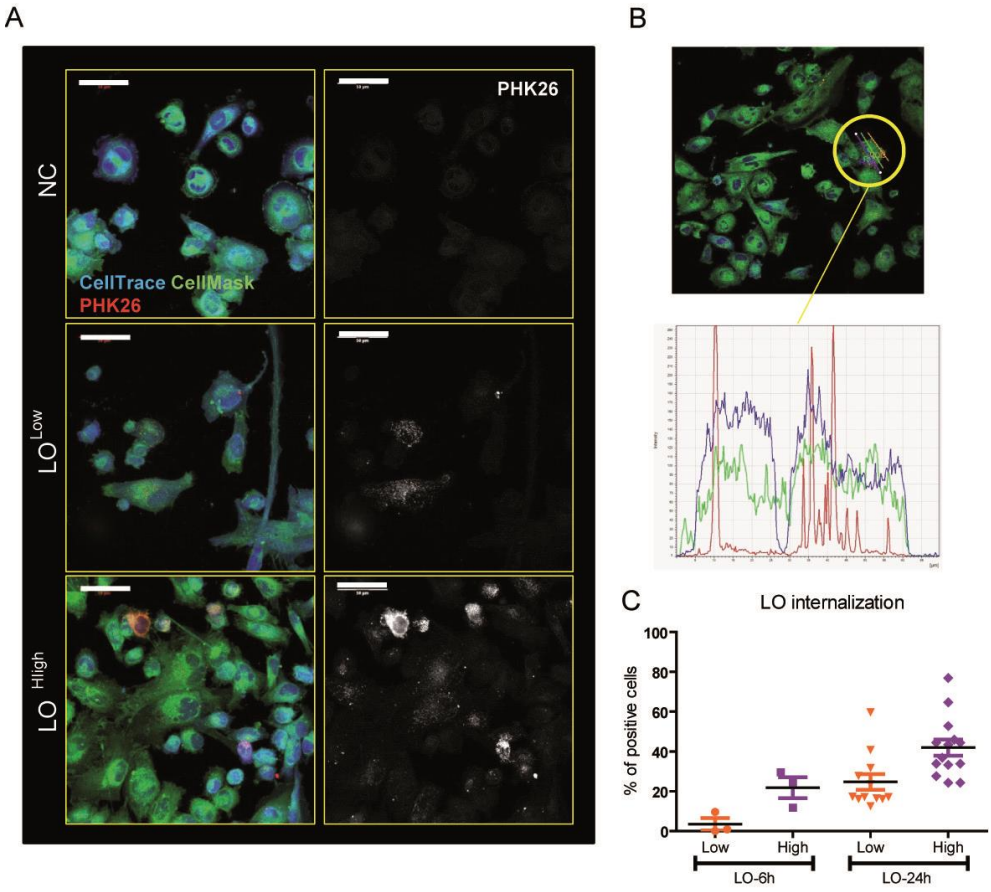

Fig. 19_LO internalization in recipient cells. Confocal image (objective 63X) of differentiated cells co-cutured with LO for 24hours (A). Representative image of Leica analysis to discriminate internalized LO (B). Quantification of cells that have internalized LO after co-culture, each dot represent an experiment (C).

A critical point in the study of exosomes internalization is their small dimension (under confocal microscope resolution). For this reason it was used flow cytometry. Exosomes were labeled with PHK26 and the equivalent of 3ml was added to differentiated cells for 2-6-24 hours. Results show that Exo^{LOW} (exosomes derived from $V1G1^{LOW}$ NS) and Exo^{HIGH} (exosomes derived from $V1G1^{HIGH}$ NS) are both internalized from 6 hours of co-culture, but at longer time, Exo^{HIGH} were internalized in a major number of cells (Fig. 20).

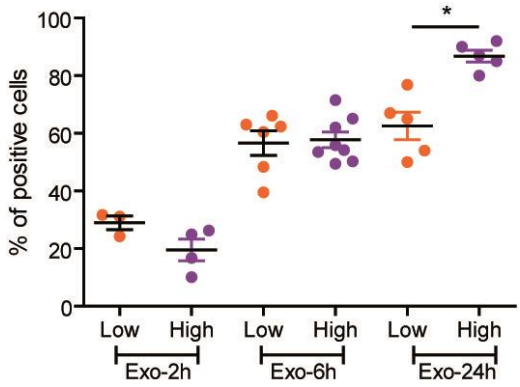

Fig.20_Exosomes internalization. Exosomes internalization in recipient cells investigated using flow cytometry (each dot represent an experiment- statistic: paired t-test).

Nanoparticle tracking analysis (NTA) on exosomes and LO derived from $V1G1^{HIGH}$ and $V1G1^{LOW}$ NS showed that there was no difference in term of concentration per ml (around $500*10^5$ in case of exosomes; Figs. 21A-B and around $1500*10^5$ in case of LO; Fig. 21C). Therefore we could conclude that inequality in term of internalization of LO was not a consequence of different extracellular vesicles concentration.

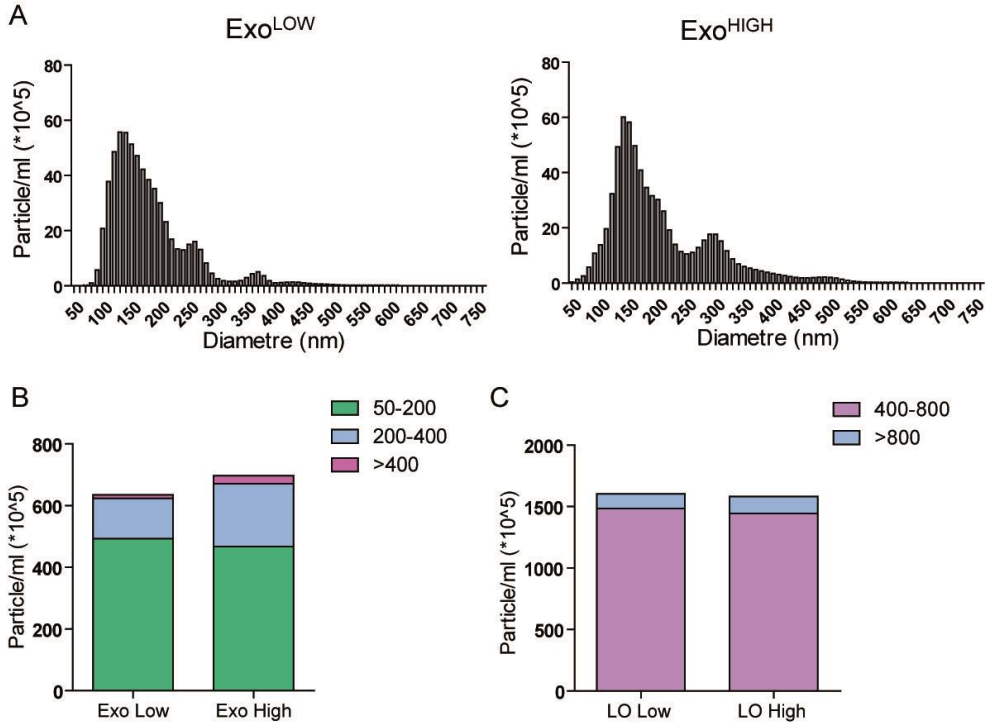

Fig.21_ Nanoparticle tracking analysis (NTA). Nanoparticle tracking analysis was performed using Nanosight NS300, vesicles distribution in size (Exo-A) and concentration per ml of vesicle in different condition (Exo-B & LO-C).

4.6 Exosomes induce cell growth and invasion of recipient cells

In order to evaluate the biological effect of extracellular vesicles produced by GBM NS on differentiated tumor cells (GBM +FBS) or non-tumorigenic margins (MG), was firstly analyzed the modulation of cell growth. To this end recipient cells were stained with Cell Trace dye and the number of division after co-culture was assessed through flow cytometry. The equivalent of 1ml of supernatant of EVs was added to recipient cells (EVs isolated from medium not conditioned was used as control). After 24hours of co-culture with exosomes, cell growth of GBM cells was strongly increased (Fig. 22A). More interestingly, Exo^{HIGH}, but not Exo^{LOW}, strongly increased number of cell division (Figs. 22B-C) and cell proliferation

(investigated by Ki67 staining; Fig. 22D) after 24hours of co-culture with GBM cells.

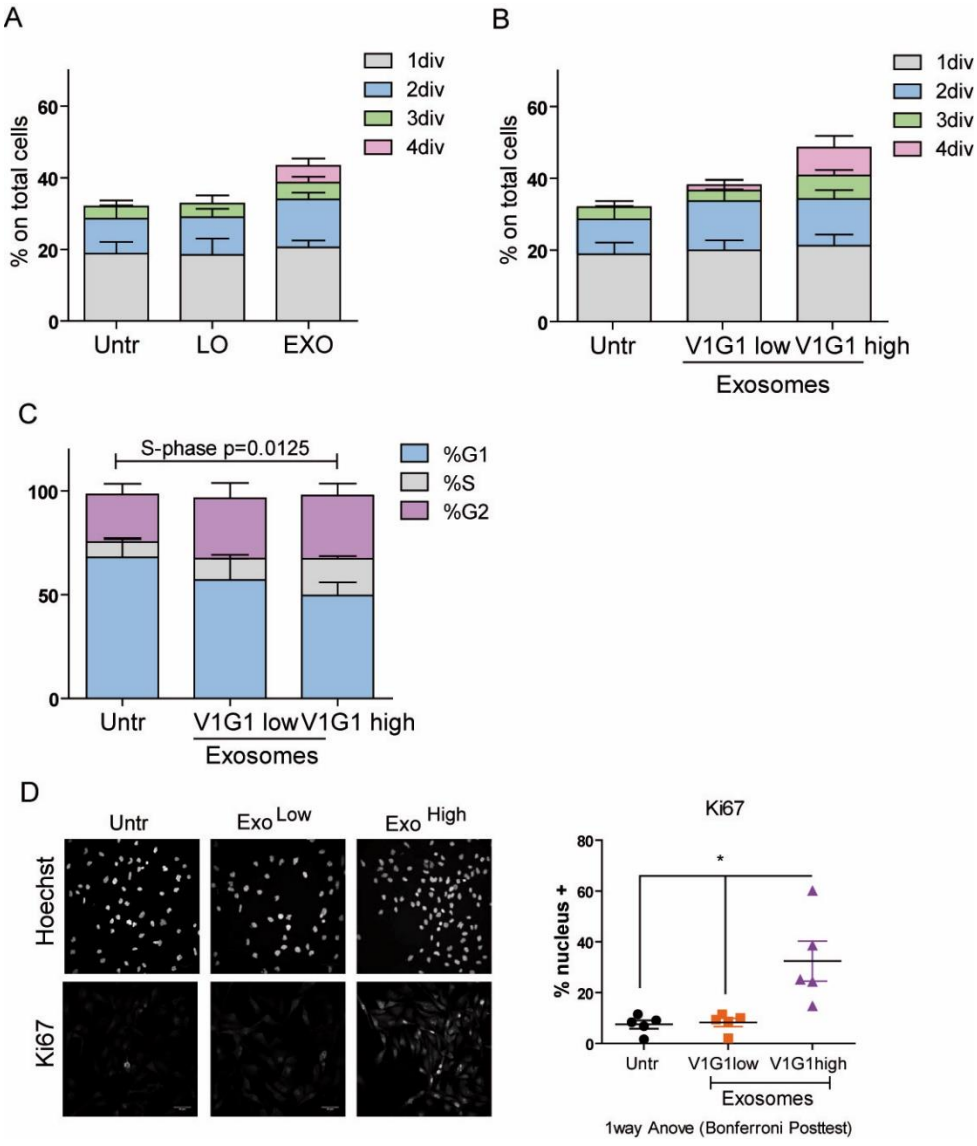

Fig.22_Co-cultere of NS-Exosomes with primary GBM cells. Cell growth was investigated using Cell Trace dye (life technologies) after 24h of co-culture (data are the average of 6 independent experiments) (A-B). Cell cycle modulation was evaluated by flow cytometry (C), t-test statistical analysis performed between S-phase at different condition (average of 6 independent experiment). Nuclear ki67

staining at basal condition and after co-culture (D – confocal image, 40X objective). Was performed 1way-Anova and Bonferroni post-test (each dot represent an independent experiment).

To evaluate whether exosomes had a similar effect also on non-neoplastic brain cultures, these experiments were performed also using tumor margins as recipient cells. In figures 23A-B is shown how exosomes not only increase cell division of MG cells, but also provide those cells with survival signals, since MG cells co-cultured with exosomes remain alive up to 17 days after exosomes supplementation whereas control MG cultures showed a mean survival time of 10 days ($p<0.01$; Fig. 23C).

Then, we evaluated cells motility of recipient cells after exosomes supplementation. After the gap was created, cells were followed for 65hours using a time-lapse microscope. Exosomes strongly increased the motility of recipient cells, particularly exosomes from $V1G1^{HIGH}$ NS, and wounds from exo-supplemented cultures were closed within 40hs whereas controls took more than 65hs (Fig. 24).

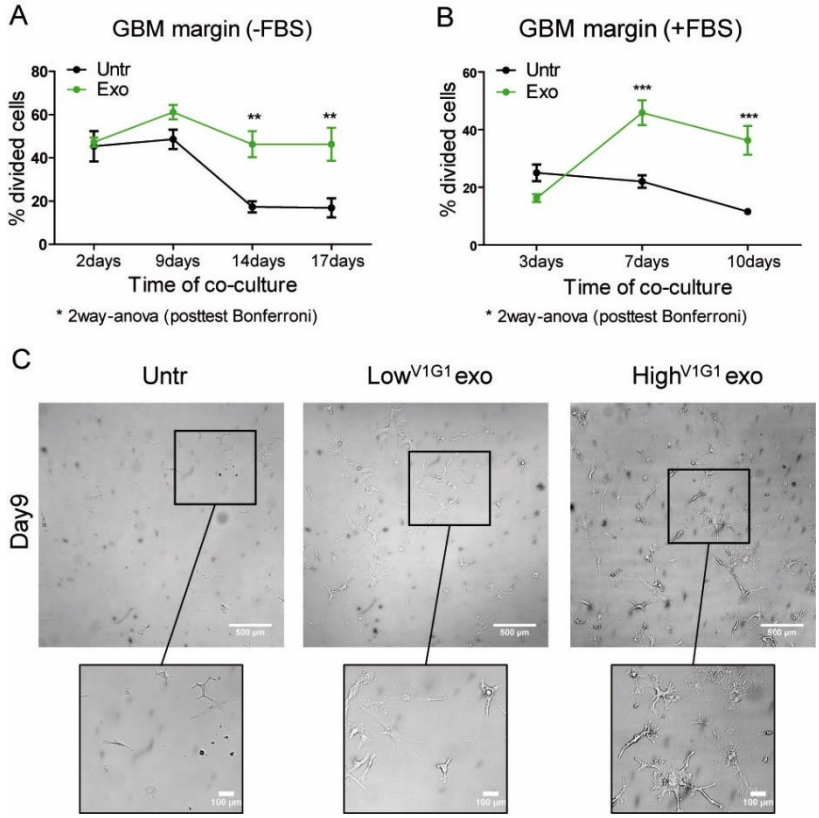

Fig.23_Exosomes co-culture with primary GBM margin cells. Number of divided cells after co-culture of MG cells maintained in differentiated (B) and undifferentiated (A) condition with exosomes (average of 4 independent experiment - 2way-anova, Bonferroni post-test). Widefiled image (objective 10X) of undifferentiated MG cells after 9days from start of co-culture with exosomes (C).

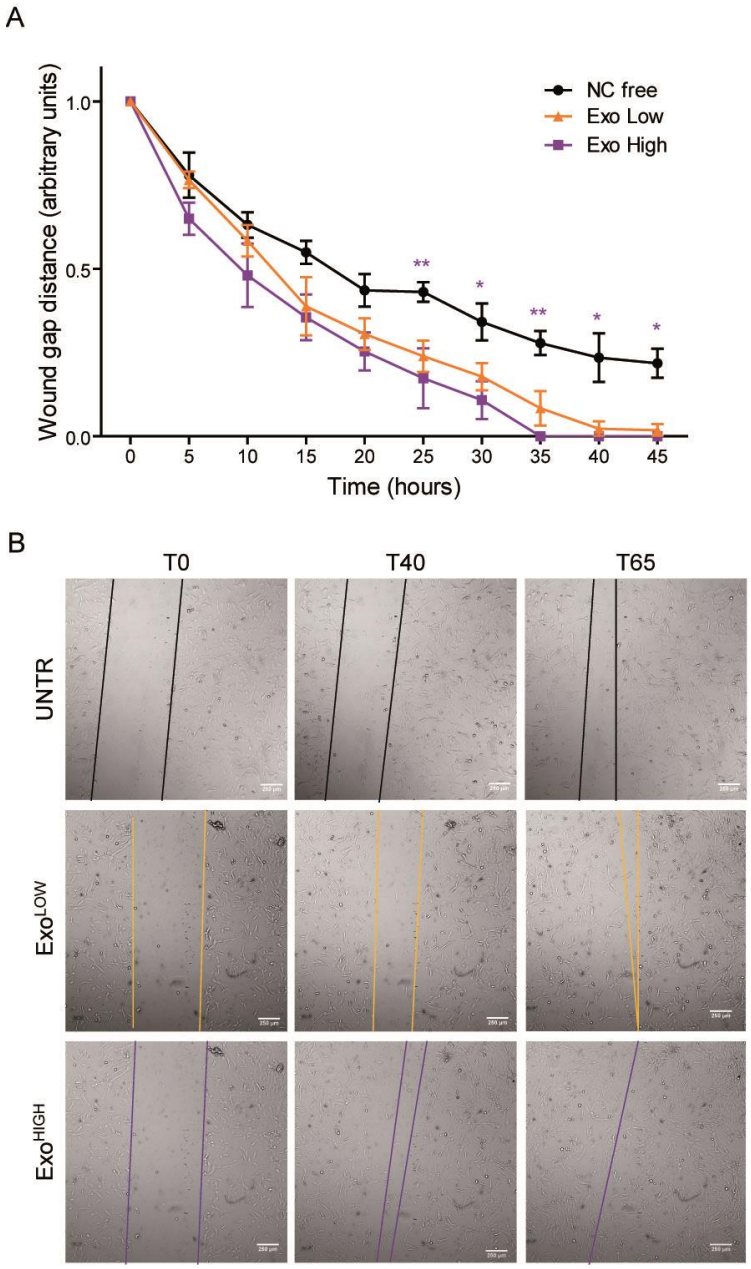

Fig.24_Cells motility. Measure of the gap (distance between the margin) at different time point (A) (average of three independent experiment – 2way Anova, Bonferroni post-test. Ctrl vs Exo^{LOW} not significant). Representative image (capture with widefield microscopy, objective 10X) of the measurement of the gap at different condition (B).

Considering that exosomes effect strongly correlates with V1G1 expression in NS producing exosomes, it was evaluated whether the inhibition of V-ATPase activity in NS, using BafA1 at the non-lethal dosage, could affect exosomes outcome on GBM and MG recipient cells. Supernatant of $V1G1^{HIGH}$ NS was collected after 24 hours in control (ctrl) and BafilomycinA1 treated (BafA1) conditions. BafA1 treatment completely reverted the exosomes effects in term of cell growth (Fig. 25A-B), cell proliferation (Fig. 25C) and cell motility (Fig. 25D). These data further confirms the central role of V-ATPase proton pump in regulating exosomes biological effect.

To ascertain that the biological effect of exosomes isolated after BafA1 treatment was not given by a different production of EVs by NS, we evaluated exosomes production, (Fig. 26A) concentration (Fig. 26 B-C) and internalization (Fig. 26D). Confirming published data [56], BafA1 treatment did not impair the ability of NS to produce different types of extracellular vesicles (Fig. 26A), but, conversely, BafA1 treatment increased the concentration of exosomes in the media (around $2000*10^5$ per ml). This result was also confirmed by NTA (Fig.26C).

Finally we could determine that after BafA1 treatment exosomes are internalized by recipient cells with a percentage of positive cells comparable to control after 24 hours of co-culture (Fig. 26D).

These data suggests that V-ATPase block by BafA1 alters exosomes content. Therefore we focused our attention on exosomes composition it term of RNA and protein contents.

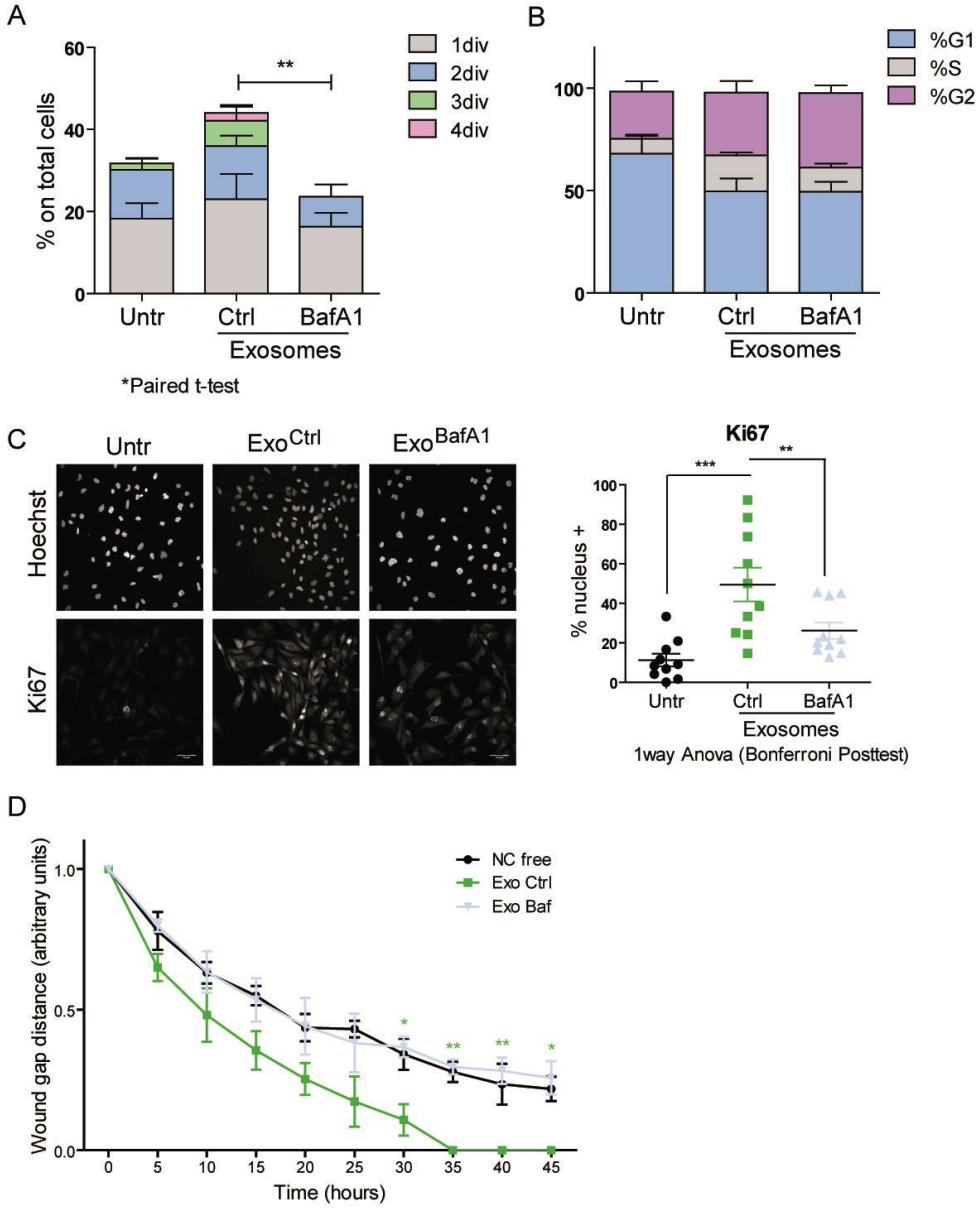

Fig.25_BafA1 treatment of NS producing cells reverts biological effect in recipient cells. Cell growth and cell cycle modulation investigated after 24h of co-culture in GBM tumor cells (n=5) (A-B; Mann-Whitney t-test of divided cells). Ki67 nuclear staining study both on GBM differentiated cells (n=3) than on MG tumor cells (n=4) (C). Cells motility investigated in GBM tumor cells (n=3) (D, 2way Anova Bonferroni posttest, asterisks referred to Exo^{CTRL} vs Exo^{BafA1}).

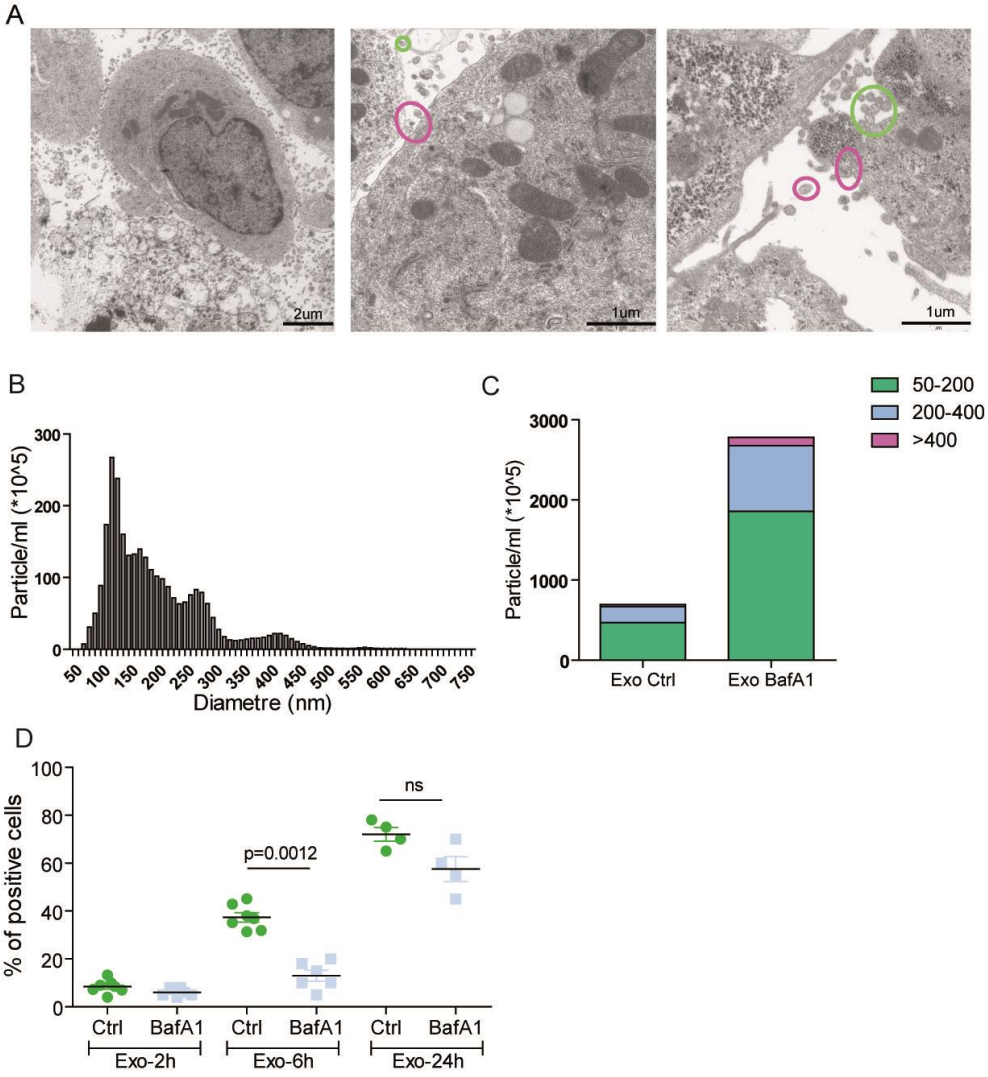

Fig.26_Characterization of exosomes after BafA1 treatment. EM image of NS after BafA1 treatment (5nM for 24 hours), scale bar=2um (image left) and 1um (center and right) (A). NTA analysis of exosomes dimension (B) and concentration (C). Exosomes internalization in recipient cells investigated using flow cytometry (D).

4.7 Exosomes co-culture induces V1G1 protein expression in recipient cells

Since in ExoCarta database[A] is described the presence of different V-ATPase subunits in exosomes from different cancer cell types, we evaluated whether NS exosomes vehiculated the V1G1 subunit. Through immunogold (Fig. 27A), western blot (Fig.27B) and FACS (Fig. 27C) analyses we could confirm that exosomes transport V1G1 protein. Specifically, V1G1 protein is present in around 30% of exosomes from $V1G1^{LOW}$ NS and after V-ATPase block by BafA1, whereas are present in around 50% of exosomes from $V1G1^{HIGH}$ NS (Fig. 27D).

To determine whether exo-V1G1 was transferred to recipient cells, we evaluated its expression modulation both at gene and protein levels after co-culture of exosomes with GBM (+FBS) or MG cultures (+/- FBS). V1G1 protein (Fig. 28 A-C) but not gene expression levels (Fig. 28B) significantly increased, both after Exo^{LOW} and Exo^{HIGH} co-culture. Genes and protein modulation of other V-ATPase subunits was also evaluated, but no modulation in recipient cells could be observed (data not shown). Interestingly, BafA1-mediated inhibition of V-ATPase activity in exo-producing NS impaired V1G1 transfer to recipient cells and no modulation of the subunit could be determined in either GBM or MG cultures at gene or protein expression levels (Fig. 28D).

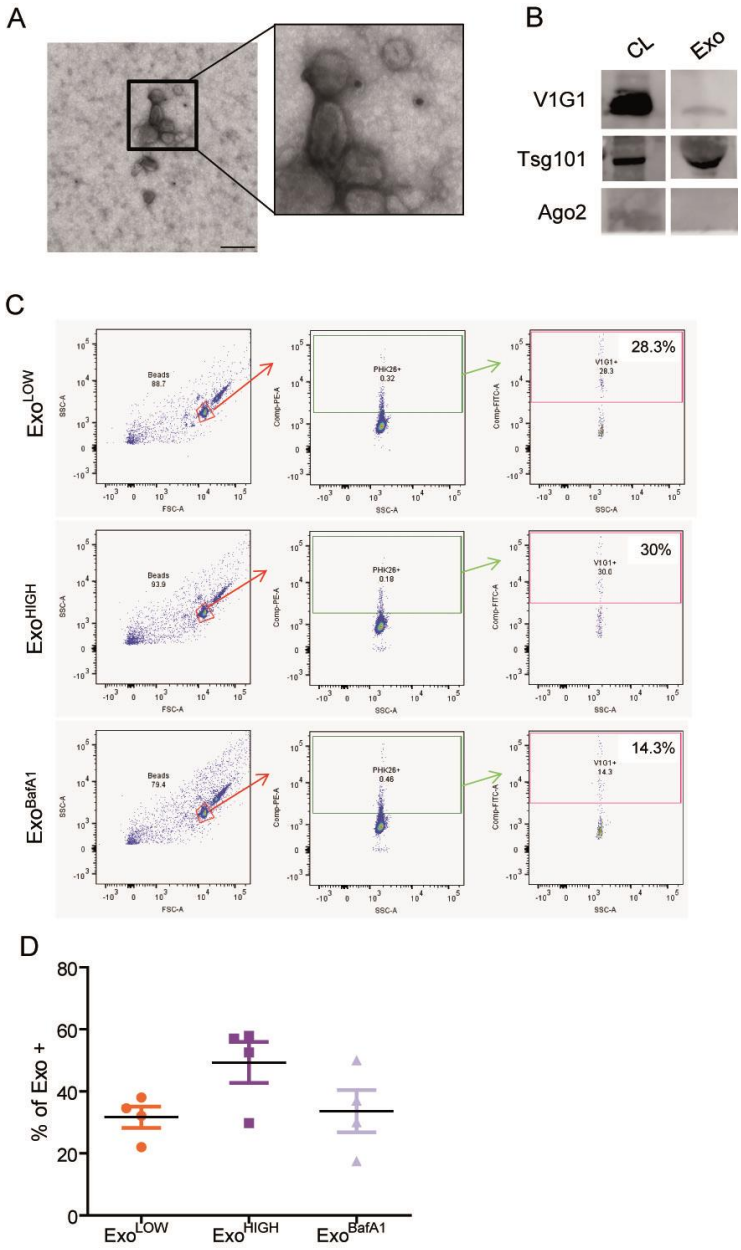

Fig.27_Exosomes carry V1G1 protein on their membrane. Representative images of immunogold performed on exosomes isolated from High V1G1 NS (scale bar= 200nm - A). Western blot of cell lysate (NS) and exosomes to investigate V1G1 protein expression (B). Exosomes was stained with PHK26 probe and then bind to CD63-coated beads in order to evaluate V1G1 staining using flow cytometry (C).

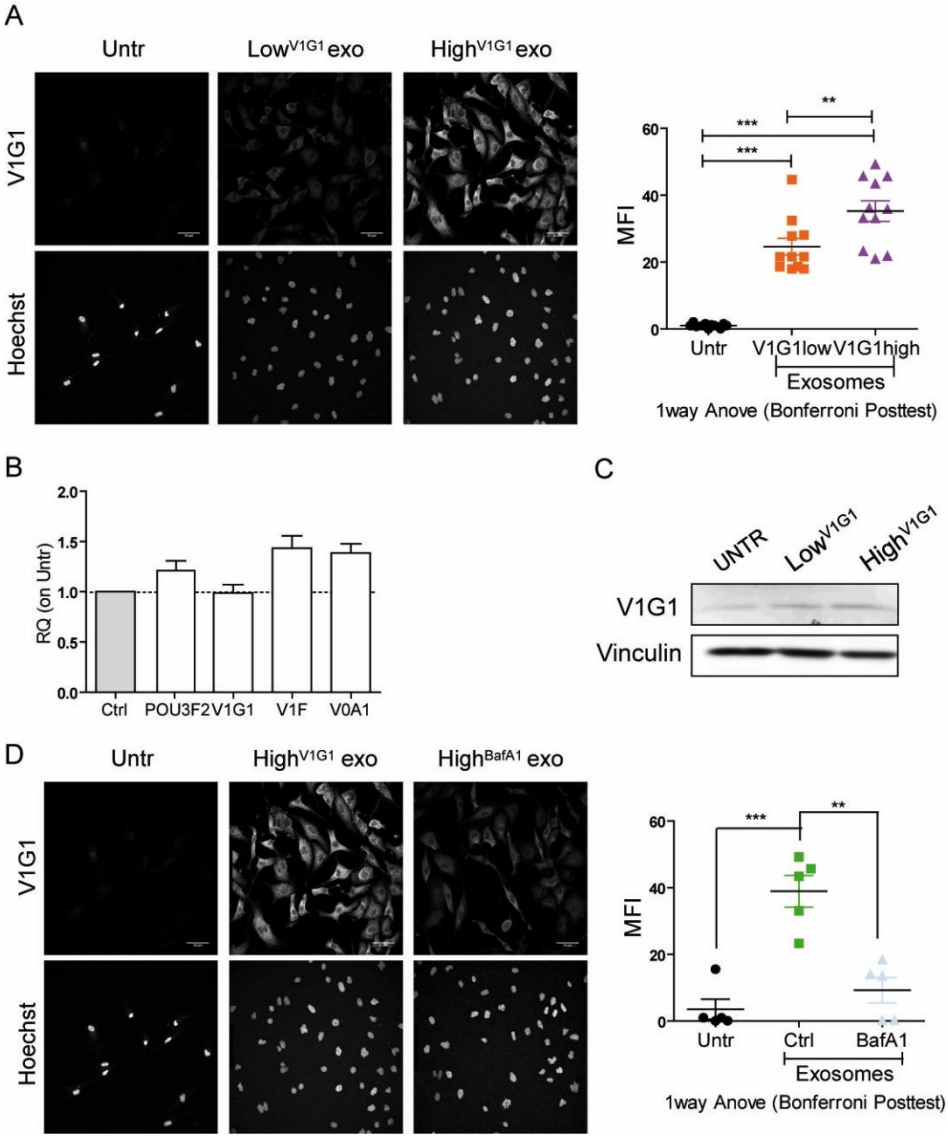

Fig.28_Co-culture with exosomes induce V1G1 protein expression in recipient cells. GBM tumor cells and MG tumor cells were co-cultured with exosomes for 24 and 48 hours respectively and V1G1 modulation was observed by immunofluorescence (A Exo^{LOW} and Exo^{HIGH} – D Exo^{BafA1}), western blot (C) and gene expression (B).

4.8 Exosomes co-culture induces MAPK pathway in recipient cells

We previously showed that V1G1 expression correlates with MAPK/Erk pathway activity in NS. Therefore we evaluated whether exosomes were able to modulate the MAPK/Erk pathway in recipient cells. In particular, the modulation of different genes and protein, associated to cell cycle and MAPK pathway, were investigated after co-culture of GBM tumor cells and MG tumor cells (+FBS) with Exo^{LOW} and Exo^{HIGH}. Heatmap analysis clearly shows how, after co-culture, there was a strong activation of all investigated genes, especially after co-culture with Exo^{HIGH} (Fig. 29A). It is interesting to notice that BCL2 was activated only after co-culture with Exo^{HIGH}. Moreover phospho-array analysis shows how, after three days of co-culture, Exo^{HIGH} strongly increased phosphorylation of Erk1/2, Stat3, AMPKα, mTOR, HSP27 and PRAS and decreased phosphorylation of GSK-3β (Fig. 29B-C), compared to Exo^{LOW} samples. These data suggest that, both Exo^{LOW} than Exo^{HIGH} activate MAPK-gene expression in recipient cells, but only after co-culture with Exo^{HIGH} there is an activation of MAPK pathway (given by modulation of different phospho protein and BCL2 activation). These results were validated by qPCR (Fig. 30A), western blot (Fig. 30B) and by immunofluorescence analysis (Fig. 30C). Moreover, IF data suggest that Erk localization to the nuclei in Exo^{HIGH} cu-cultured samples (Fig. 30C) could be responsible of the Bcl2 up-regulation at transcriptional level.

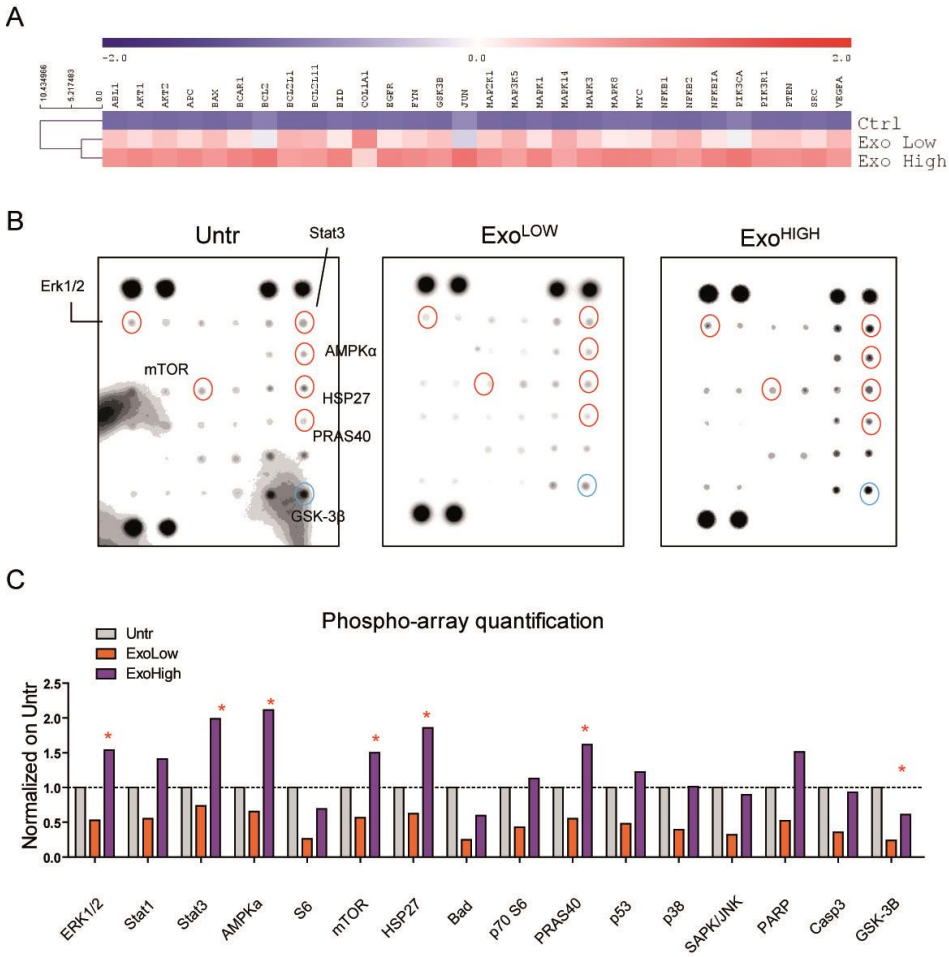

Fig.29_MAPK pathway activation in recipient cells after co-culture with Exo-High^{V1G1}. Unsupervised heatmap (Average Euclidean metric) of GBM tumor cells at control condition and after co-culture with Exo^{LOW} and Exo^{HIGH} (A). Phospho-array quantification (B) and representative image (C) of MG tumor cells at control condition and after co-culture with exosomes. For this purpose, *TaqMan® Array Human Molecular Mechanisms Of Cancer 96-well plate* (Life Technologies) and *PathScan Intracellular Signaling Membrane Array Kit* (Cell Signaling) were used.

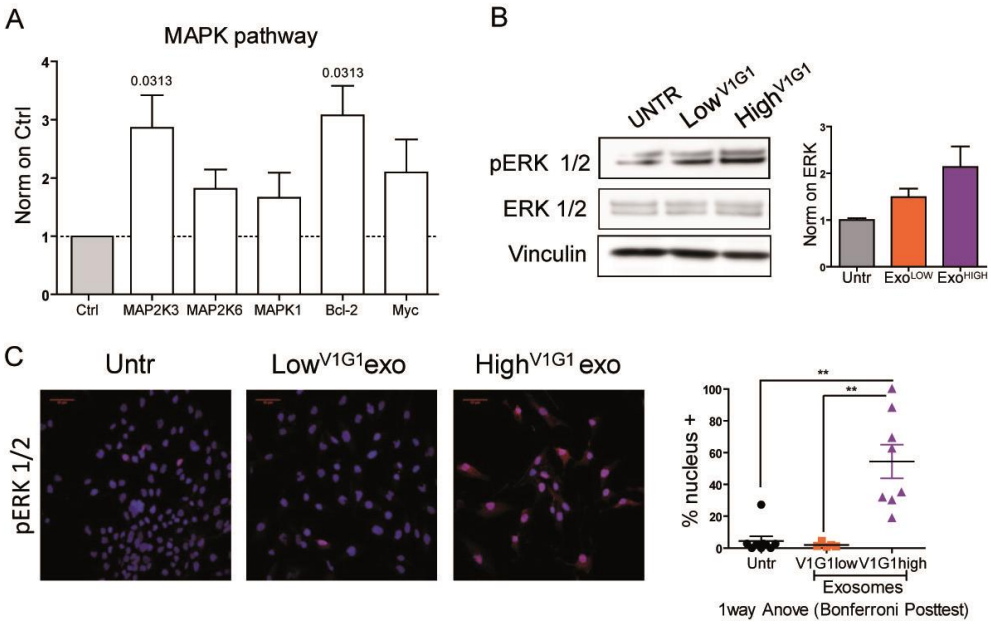

Fig.30_ MAPK pathway activation in recipient cells after co-culture with Exo-High^{V1G1}. Validation of MAPK genes using TaqMan quantitative real-time PCR (A). Western blot analysis of pERK and total ERK after co-culture and quantification (B). Representative immunofluorescence image (capture at 40X objective) of MG tumor cells (+FBS) after co-culture and quantification of nuclear traslocation of pERK (n=6) (C).

Since exosomes isolated from V1G1^{HIGH}-NS after BafA1 treatment did not induce a biological effect, we evaluated whether the treatment abrogated the effect on MAPK modulation. In line with our previous observation, BafA1 treatment of NS producing exosomes completely blocks the ability of Exo^{HIGH} preparation to activate the MAPK pathway in recipient cells in terms of gene expression (Fig. 31A), protein phosphorylation (Fig. 31B-C-D) and Erk1/2 translocation (Fig. 31E).

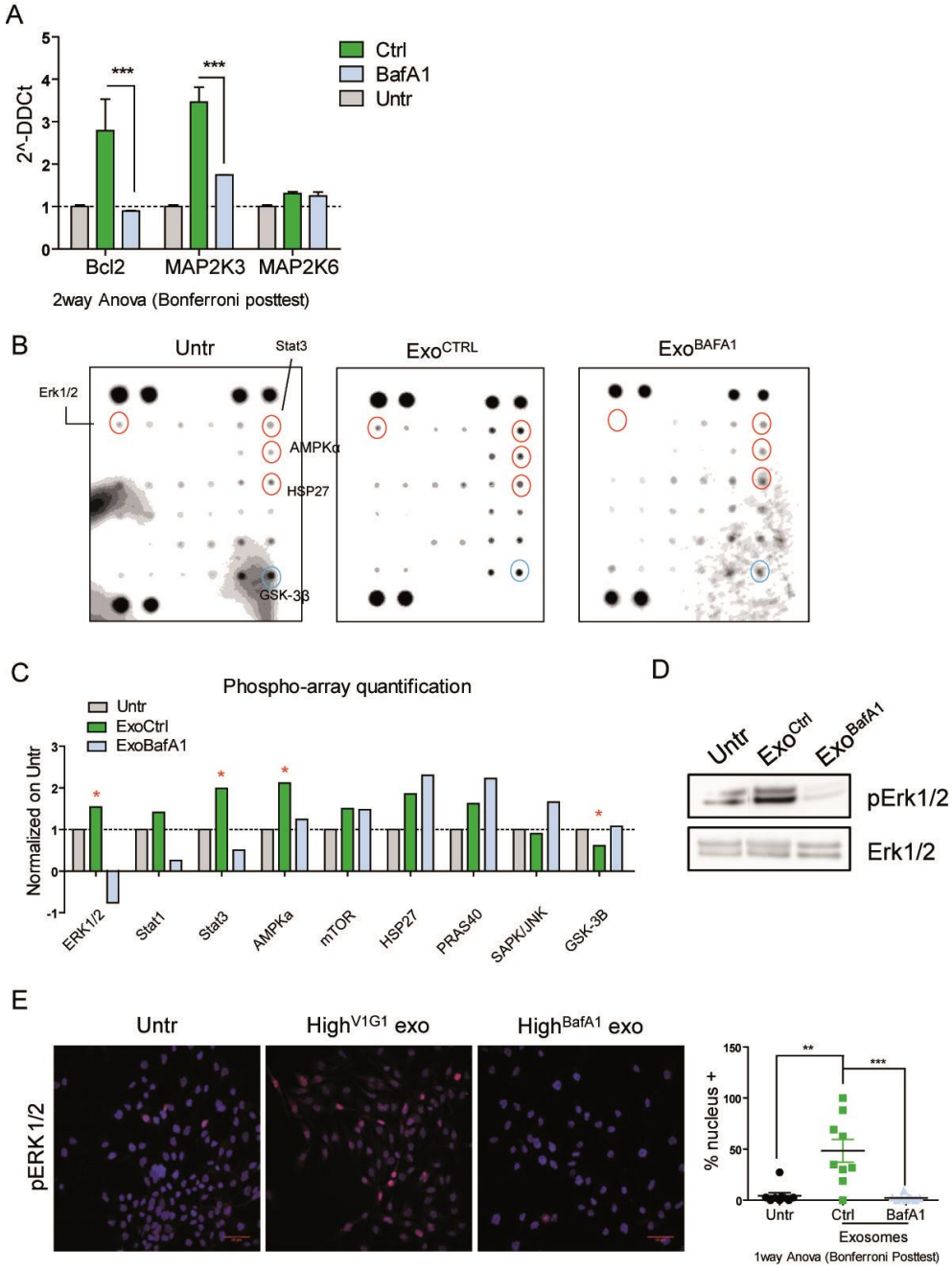

Fig.31_BafA1 treatment of NS reverts the effect in recipient cells. Quantitative Real Time PCR of modulated MAPK genes after co-culture with Exo^{HIGH} and Exo^{BafA1} (A). Phospho-array quantification (C) and representative image (D) of MG tumor cells at control condition and after co-culture with exosomes. Western blot

analysis of pERK and total ERK after co-culture (D). Representative immunofluorescence image (capture at 40X objective) of MG tumor cells (+FBS) after co-culture and quantification of nuclear traslocation of pERK (n=5) (E).

4.10 miRNA exo-signalling, but not mRNA, correlates with V-ATPase expression in NS producing exo

It is known that exosomes can transport mRNA and/or miRNA. To determine how MAPK/Erk was modulated by exosomes in recipient cells we analyzed both mRNA and miRNA contents of our exosomes preparations. Looking at MAPK- or Akt related mRNA, no difference could be observed between Exo^{LOW} and Exo^{HIGH} mRNA content (Fig. 32).

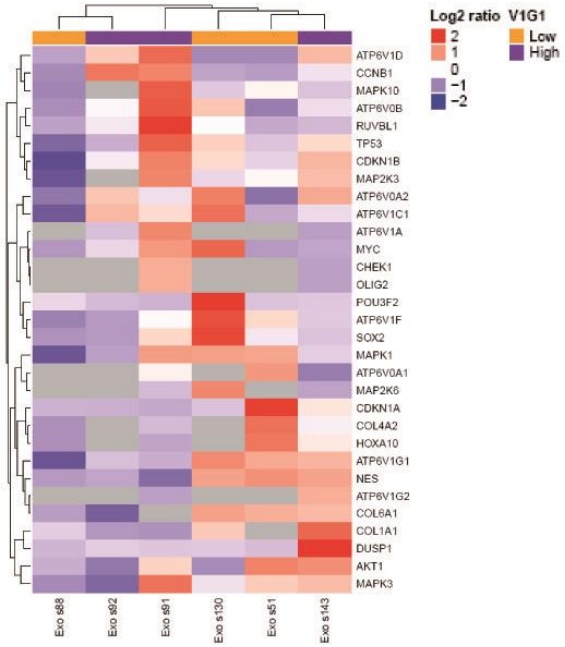

Fig.32_mRNA vehiculated in exosomes. Heatmap shows unsupervised hierarchical clustering (Euclidean complete metric was used for sample and gene) of mRNA content in exosomes from NS with high or low-V1G1 expression. Blue square, under-expressed gene; red square, over-expressed gene.

Then, the miRNA profiling of NS and of NS-derived exosomes at different conditions was investigates. As expected NS miRNA content was higher than exo-miRNA content (not shown). In exosomes about 150 were expressed above threshold levels. By unsupervised hierarchical clustering (Fig. 33A) and principal component analysis (Fig. 33B), we could highlight that miRNA content in exosomes correlated with V-ATPase expression of NS. This analysis also showed that Exo^{LOW} preparation expressed higher levels of miRNA. By SAM analysis we identify 45 significantly different miRNA between Exo^{LOW} and Exo^{HIGH} (Fig. 33C and Table 5).

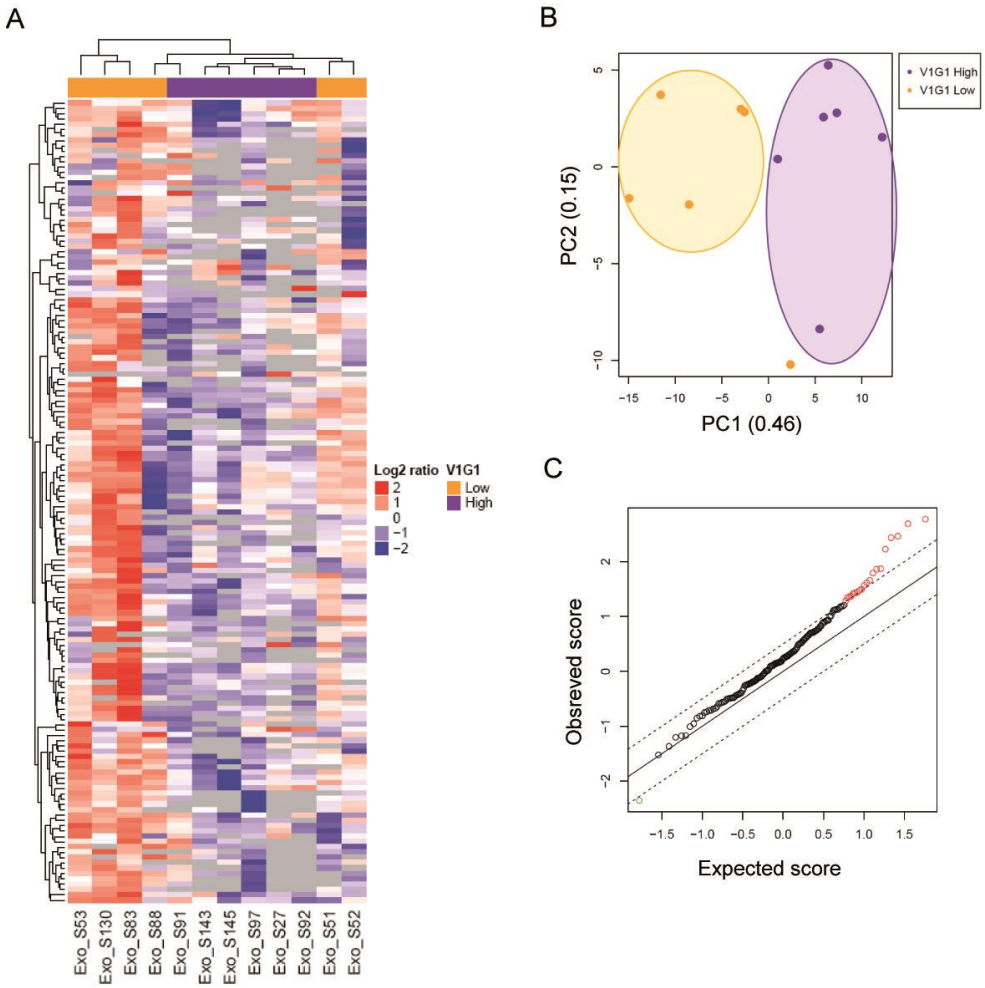

Fig.33_miRNA vehiculated in exosomes. (A) Heatmap shows unsupervised hierarchical clustering (linkage complete, metric manhattan) of miRNA content in exosomes from NS with high or low-V1G1 expression (n=12). Blue square, under-expressed gene; red square, over-expressed gene. Spheres V1G1 over expression characterized (purple bars) produce exosomes with lower miRNAs levels compared to exosomes derived V1G1 down regulated spheres (orange bars), miRNAs (n=151). (B) Principal component analysis (PCA) of exosomes (Orange dots= Exo^{LOW} – Purple dots= Exo^{HIGH}). (C) Statistical analysis of microarray (SAM) plot of miRNA differentially expressed between over and lower expressed V1G1 subunit exosomes. miRNAs downregulated and upregulated in the Exo^{LOW} are shown in green and red, respectively (n=45). FC>1log (abs), median false discovery rate (FDR)< 0.05; q.value < 0.10.

Gene Name	Score(d)	FC (HM)	q-value(%)
hsa-miR-191-5p	-1.70	-1.16	1.05
hsa-miR-320a	-3.22	-1.55	0.00
hsa-miR-34a-5p	-1.17	-1.62	2.74
hsa-miR-30c-5p	-1.64	-1.65	1.05
hsa-miR-30b-5p	-1.69	-1.74	1.05
hsa-miR-93-5p	-1.59	-1.81	1.05
hsa-miR-19b-3p	-1.97	-1.86	0.00
hsa-miR-16-5p	-2.63	-2.11	0.00
hsa-miR-29a-3p	-1.73	-2.11	1.05
hsa-miR-9-5p	-1.44	-2.12	1.05
hsa-miR-195-5p	-1.62	-2.13	1.05
hsa-miR-106a-5p	-2.67	-2.16	0.00
hsa-miR-127-3p	-1.29	-2.16	2.74
hsa-miR-24-3p	-1.84	-2.16	0.00
hsa-miR-374b-5p	-2.27	-2.39	0.00
hsa-miR-25-3p	-1.37	-2.45	1.96
hsa-miR-21-5p	-1.48	-2.46	1.05
hsa-miR-193b-3p	-2.16	-2.48	0.00
hsa-miR-106b-5p	-2.12	-2.49	0.00
hsa-miR-140-5p	-1.32	-2.55	2.74
hsa-miR-574-3p	-2.07	-2.61	0.00
hsa-miR-20a-5p	-1.95	-2.62	0.00
hsa-let-7d-5p	-1.31	-2.63	2.74
hsa-miR-374a-5p	-1.64	-2.64	1.05
hsa-miR-17-5p	-2.46	-2.69	0.00
hsa-miR-28-3p	-1.97	-2.72	0.00
hsa-miR-125b-5p	-1.69	-2.73	1.05
hsa-miR-26a-5p	-1.58	-2.76	1.05
hsa-miR-186-5p	-2.98	-2.81	0.00
hsa-let-7g-5p	-1.78	-2.91	0.00
hsa-miR-9-3p	-1.97	-3.00	0.00
hsa-miR-454-3p	-1.79	-3.03	0.00
hsa-miR-885-5p	-2.34	-3.09	0.00
hsa-let-7b-5p	-3.00	-3.12	0.00
hsa-miR-100-5p	-1.55	-3.12	1.05
hsa-miR-151a-3p	-1.90	-3.34	0.00
hsa-miR-30e-3p	-1.69	-3.37	1.05
hsa-miR-15b-5p	-1.76	-3.37	0.00
hsa-let-7e-5p	-2.30	-3.46	0.00
hsa-miR-132-3p	-1.18	-3.54	2.74
hsa-miR-30a-3p	-1.61	-3.64	1.05
hsa-miR-99a-5p	-1.69	-4.33	1.05
hsa-miR-30a-5p	-1.79	-4.35	0.00
hsa-miR-222-3p	-1.57	-4.72	1.05
hsa-miR-135b-5p	-1.57	-5.07	1.05

Table5_45 SAM selected miRNAs in exosomes.

We then looked at these miRNAs in the NS that generated the exosomes, but spheres and exosomes clustered in two different branches (Fig. 34A). Moreover PCA analysis demonstrate that miRNA profiling clearly distinguish (by PC1) V1G1^{HIGH}-NS from corresponding Exo^{HIGH}. Instead

V1G1^{LOW}-NS and Exo^{LOW} partially overlap (Fig. 34B). Finally, focusing only on 45 miRNA found after SAM analysis in exosomes, unsupervised clustering (Fig. 35) confirm that miRNA content in exosomes (Fig. 35A) doesn't correlate with cells content (Fig. 35B); on the contrary in NS miRNA profile is the opposite of exosomes, with an higher expression in V1G1^{HIGH}-NS.

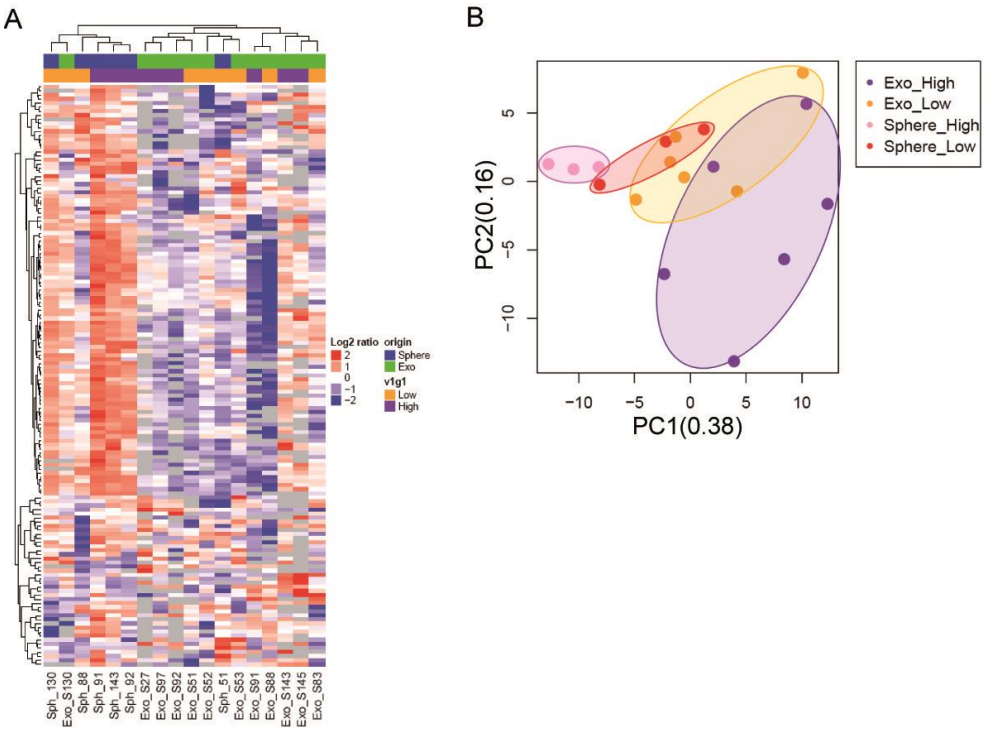

Fig.34_miRNA in exosomes and neurospheres. (A) Heatmap shows unsupervised hierarchical clustering (linkage complete, metric pearson) of exosomes (green bars) and NS (blue bars) derived miRNAs. NS and exosomes clustered in two different branches. Furthermore, independently of V1G1 subunit expression, the NS shows higher miRNAs expression compared with exosomes. (B) PCA of exosomes and NS (Pink dots= HighV1G1 NS – Red dots= LowV1G1 NS – Orange dots= Exo^{LOW} – Purple dots= Exo^{HIGH}).

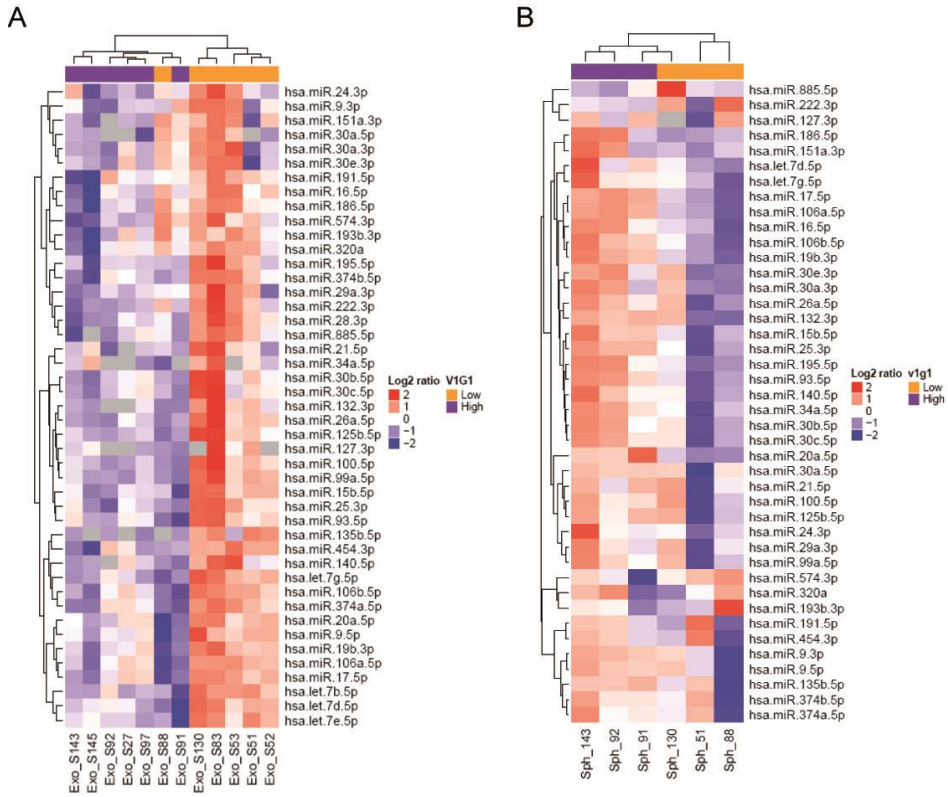

Fig.35_Different expression of 45 SAM selected miRNAs in exosomes and NS. (A) Heatmap shows unsupervised hierarchical clustering (linkage complete, metric manhattan) of Exo-miRNA and reveals a higher miRNAs expression in exosomes V1G1^{LOW} (orange bars). (B) Heatmap shows unsupervised hierarchical clustering (linkage complete, metric manhattan) of NS-miRNA and reveals an over-expression of miRNAs in V1G1^{HIGH}-NS (purple bars).

By bioinformatics analysis of the predicted gene targets of 45 selected miRNA we could determine an enrichment of genes associated to cell cycle (62 out of 95) and to MAPK pathways (67 genes; Fig 36).

miRNA associated to MAPK pathway were validated through quantitative real time PCR in a different subset of exosomes derived from NS (n=8) and 10 miRNA were confirmed as strongly up regulated in Exo^{LOW} compared to Exo^{HIGH} (Fig. 37A). Moreover, it was investigated whether miRNA levels were modulated after BafA1 treatment. Figure 37B shows that BafA1

treatment up regulates miRNA exosomes content, with level comparable to Exo^{LOW} samples.

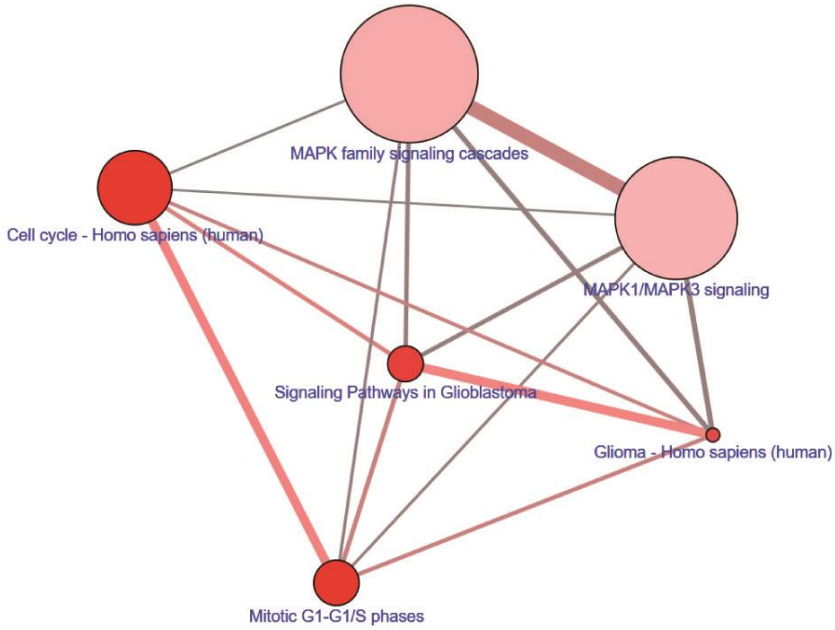

Fig.36_Gene target pathway. Network of principal pathway targeted by significant miRNA (n=45) (CPDB software, over-representation analysis, each node represents a separate pathway whose member list size (number of genes contained) and P-value are encoded as node size and node color, respectively.

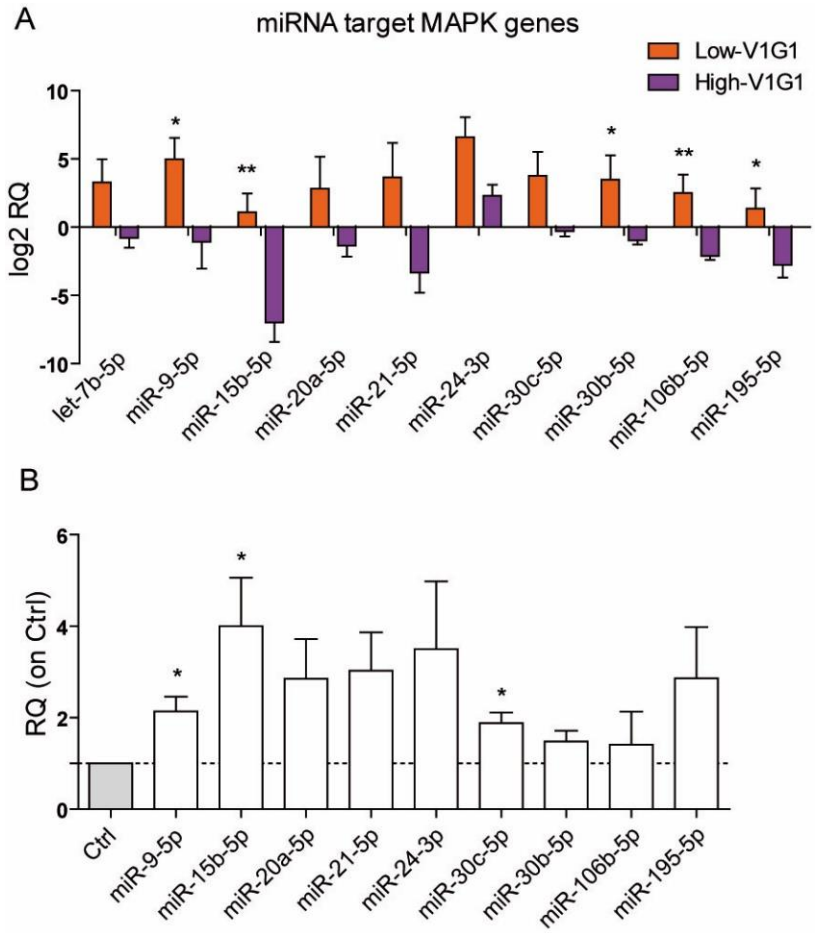

Fig.37_miRNA validated in Real Time PCR. Quantitative Real Time PCR of miRNA isolated from exosomes at basal condition (n=4 Exo^{LOW} and 4 Exo^{HIGH}) (A) and after BafA1 treatment of NS (n=4) (B). T-test was performed for statistic.

Finally, we evaluated whether that miRNA validated by qRealTime PCR, were modulation in recipient cells. Six out of 10 miRNAs (namely miR-9-5p, miR-15-5p, miR-21-5p, miR-30b-5p, miR-30c-5p, miR-195-5p) resulted up-regulated in GBM and MG cultures only after supplementation with the Exo^{LOW} and not with Exo^{HIGH} or Exo^{BafA1} preparations (Fig. 38).

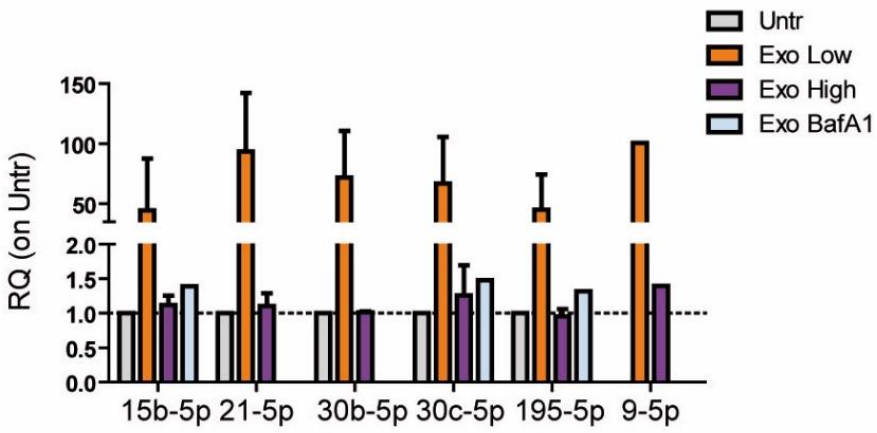

Fig.38_Co-culture with Exo^{LOW} increase miRNA expression in recipient cells. MG tumor cells (n=3) and GBM tumor cells (n=2) were co-cultured with exosomes for 48 and 24 hours, respectively. miRNA level were investigated through quantitative Real Time PCR, and exogenous miRNA (spike-in or miR-39) was used as reference.

4.11 miRNA exo-signalling blocks MAPK pathway activation in Exo-Low^{V1G1}

Based on our data, we envisioned a model in which miRNA vehiculated by Exo^{LOW}, bind MAPK/Erk transcripts after internalization in recipient cells, thus blocking their translation and, as a consequence, the signaling pathway (Fig. 39).

To confirm our model, first we confirmed the data using another V-ATPase inhibitor, such as Concanamycin A (ConcA). As expected, ConcA at dosages able to decrease lysosomal acidification without affecting cell viability (Fig. 40A,B) increased miRNAs (namely miR-9-5p, miR-21-5p, miR-30b-5p, miR-30c-5p, miR-195-5p) (Fig. 40C). This result further supports the role of V-ATPase in selecting miRNAs that will be loaded in MVB-generating exosomes.

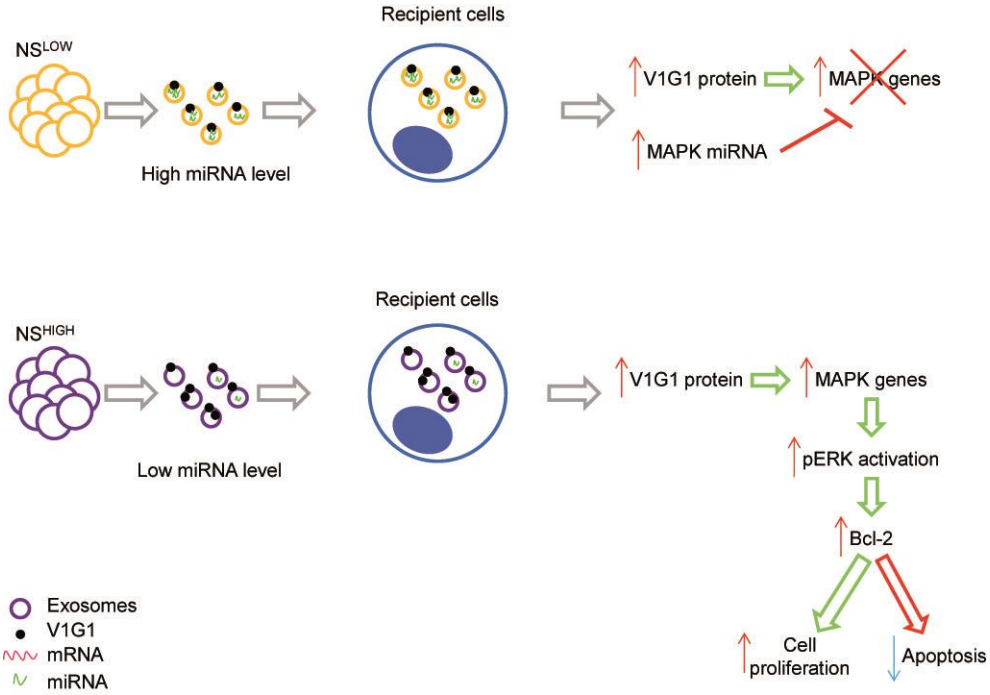

Fig.39_Proposed model of exosomes activity.

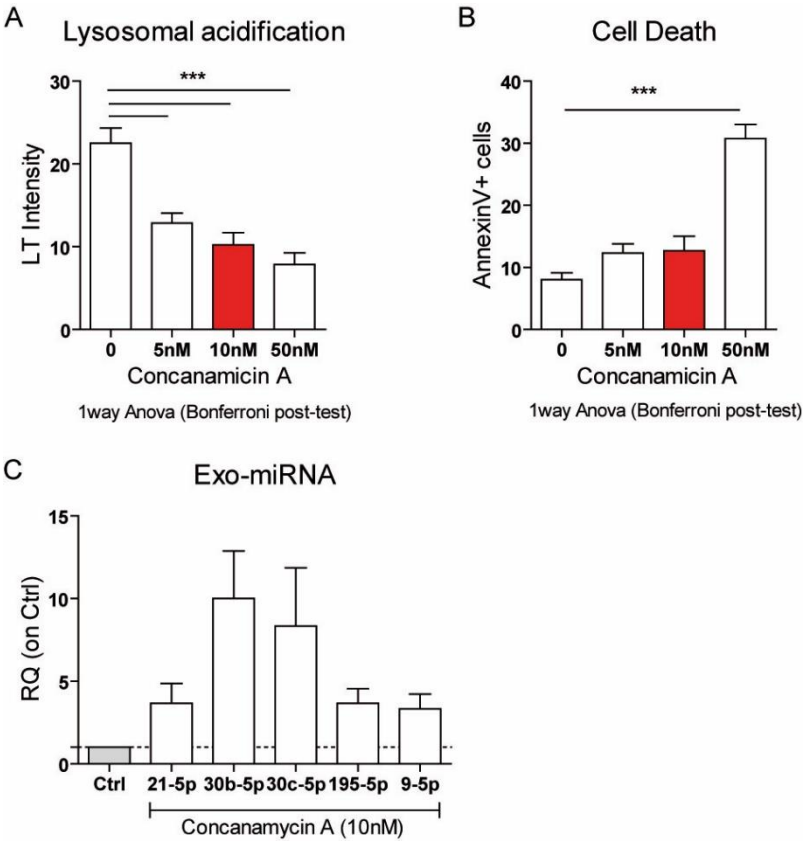

Figure 40_Lysosomal acidification was investigated using lysotracker probe after ConcA treatment (A). Cell death was investigated as AnnexinV positive cells (percentage of positive cells; B). Quantitative RealTime PCR of miRNA content in exosomes produced by HighV1G1 NS after ConcA treatment (C).

5. DISCUSSION

5.1 V-ATPase proton pump sustain glioma stem cells niche

V-ATPase proton pump was recently found up-regulated in various type of tumors, in particular it has been described to sustain the cancer stem cell niche [57] and its activity appears to be required by ovarian or breast cancer cells to invade and metastasize [53, 58, 59], or to activate oncogenic signalling [22, 24, 60, 61]. In a previous work, published by our group (Di Cristofori et al., 2015 [62]), we demonstrated that V-ATPase G1 is a novel marker of poor prognosis for glioblastoma patients and that it is selectively up-regulated in GSC. In this thesis, we confirmed that V-ATPase proton pump, in particular ATP6V1G1 subunit, has a central role in maintenance GSC viability, tumorigenicity and stem cell factors expression. In particular, in this work we got novel insights into the role of ATP6V1G1 subunit in maintenance glioma stem cells niche, investigating the involvement of associated signalling pathway. Firstly, we demonstrated that ATP6V1G1 gene expression classified NS in two different groups, characterized by different stemness and aggressive features, such asstem genes expression, clonogenicity, invasiveness, and MAPK/Erk pathway activation. Moreover, the inhibition of V-ATPase activity by BafA1 significantly reduced motility and clonogenicity of NS without affecting cell viability. On the contrary, in differentiated cells BafA1 treatment was ineffective.

Glioma stem cells are involved in therapeutic resistance and disease relapse in glioblastoma patients, with consequent life expectancy of about 14-16 months. For this reason, it is crucial to find new drugs able to specifically target the GSC niche. Therefore new information and study

regarding the molecular alterations that characterize different subsets of high-grade glioma are necessary. In this scenario, our work sheds light into a novel mechanism exploited by cancer stem cell to survive and invade, which relies on V-ATPase pump deregulation. Importantly, the V-ATPase could be a druggable target and directed drugs are currently under preclinical development [63, 64].

In this work we also demonstrated that in GBM NS there is a strong correlation between V1G1 up-regulation and MAPK/Erk pathway activation, whereas there is no association with other cancer pathway (e.g. Notch or PI3K/Akt/mTOR pathways). Indeed we demonstrated that V-ATPase impairment, using Bafilomycin A1, causes down-regulation of MAPK/Erk pathway.

5.2 V-ATPase proton pump regulates exosomes signalling in glioma stem cells

Recent evidences highlighted that GBM secreted microvesicles, particularly exosomes and large oncosomes, play a major role in the cross-talk between tumor cell and non-neoplastic parenchyma [34, 46, 65]. V-ATPase might regulate intra- and extra-cellular milieu by acidification and by modulating protein trafficking in organelles, such as endosomes and lysosomes [30, 53, 54]. Indeed, in ExoCarta database, V-ATPase subunits are described in exosomes from different cancer cell types [56].

Therefore in this thesis we focused on the possible role of V-ATPase proton pump in regulating extracellular vesicles signalling in glioblastoma, in particular on exosomes. Initially, we demonstrated that GBM NS can product different types of extracellular vesicles, such as exosomes and large oncosomes, independently from V-ATPase G1 expression level. Nevertheless, exosomes produced by V1G1^{HIGH}-NS have a higher ability to

be internalized in recipient cells. Since it is well know that EVs can influence the microenvironment through the horizontal transfer of bioactive molecules [22, 34, 40, 66-68], we investigated EVs effects on two different types of recipient cells. In particular, we observed that Exo^{HIGH} strongly increase cell growth and cell motility both in non-neoplastic cultures from tumor margins (MG) and primary tumor cultures from GBM tissues. Moreover, our data suggest that V1G1 expression in NS producing exosomes correlates with biological effect on recipient cells, such as activation of MAPK/ERK pathway. In line with this, the treatment of $V1G1^{HIGH}$ NS with BafA1 reverts the exosomes-mediated biological effects in recipient cells.

Interestingly both Exo^{LOW} and Exo^{HIGH} carry V1G1 protein on their surface, and V1G1 expression decreases in exosomes derived from NS treated with BafA1. Furthermore Exo^{LOW} and Exo^{HIGH}, but not Exo^{BafA1}, induce V1G1 expression in recipient cells, but only Exo^{HIGH} activates the MAPK/Erk pathway in recipient cultures.

To better understand the V1G1-MAPK/ERK signaling axe, we hypothesized that exo-miRNAs could play a role, as previously demontrated in other cancer context [65, 66, 69-72]. Accordingly we profiled the miRNome of exosomes prepared from V1G1 High and Low NS. Around 150 miRNAs were present in exosomes (whereas NS expressed 388 miRNAs). Interestingly we found that exosomes-miRNA signaling inversely correlates with V1G1 expression in NS. In particular, Exo^{LOW} vehiculates a higher number of miRNAs compared to Exo^{HIGH}. Remarkably, when we investigated the expression of these miRNAs in NS, we found that their expression is higher in $V1G1^{HIGH}$ NS compared to $V1G1^{LOW}$. Altogether these data suggest that $V1G1^{HIGH}$ NS selectively do not vehiculate these miRNAs in exosomes.

Bioinformatics and in vitro analyses of the miRNAs targets revealed that the majority of Exo^{LOW}-miRNAs are directed towards MAPK pathway members and cell cycle genes. These data suggest that Exo^{LOW}-miRNAs, after co-culture, are internalized by recipient cells where they repress expression of genes related to the V-ATPaseG1/ERK signaling.

Further work is required to better investigate how V-ATPase activity and modulation may regulate exosomes content and to study the involvement of other V-ATPase subunits in regulating exosomes signaling.
Moreover, the study analysis of specific miRNAs in glioma patients serum could provide translational insights into disease monitoring. The heterogeneous nature of GBM may contribute to the variation in survival observed in GBM patients with regards to response to the current clinical treatments. In this scenario, one possible approach would be to investigate the presence of specific miRNAs in exosomes isolated from human serum as tumor biomarker for tracking cancer progression through a ‘liquid biopsie’ approach.

6. CONCLUSION

In this work we supported and confirmed the hypothesis that ATP6V1G1 expression in human glioma stem cells confers proliferative advantage, it is required for cancer stem cell migration and invasion, and sustains cancer cell tumorigenicity. Moreover, we determined the central role of V1G1 subunit in glioma stem cells, in influencing the tumor microenvironment throgh the horizontal transfer of bioactive molecules such as exosomes and large oncosomes. To conclude, these data identify V-ATPase as an important driver of gliomagenesis, and a novel, actionable therapeutic target for disease intervention.

Moreover, in this thesis we documented the association between V-ATPase (in particular the V1G1 subunit) and the MAPK/Erk pathway activation. In fact, we demonstrated that V1G1 up-regulation in recipient cells (vehiculated by exosomes) induces the transcription of different MAPK associated genes. High level of V1G1 in NS producing exosomes causes a reduction of MAPK-associated miRNA internalized in exosomes. Indeed only the co-culture with Exo^{HIGH} preparation induces the activation of the MAPK/ERK pathway, with the translocation of phosphorylated Erk in the nuclei of recipient cells and, as a consequence, the transcription of Bcl-2. On the contrary and further supporting our model, the co-culture with Exo^{LOW} up-regulates MAPK-directed miRNAs in recipient cells.

Given this data, we can conclude that V-ATPase is a novel player in glioma stem cell pathobiology and signaling.

7. BIBLIOGRAPHY

1. Louis, D.N., et al., *The 2007 WHO classification of tumours of the central nervous system.* Acta Neuropathol, 2007. **114**(2): p. 97-109.
2. Neuropathology Group of Pathology Branch of the Chinese Medical, A., *[World Health Organization classification of tumours of the central nervous system: a summary].* Zhonghua Bing Li Xue Za Zhi, 2016. **45**(11): p. 745-747.
3. Cimino, P.J., et al., *Multidimensional scaling of diffuse gliomas: application to the 2016 World Health Organization classification system with prognostically relevant molecular subtype discovery.* Acta Neuropathol Commun, 2017. **5**(1): p. 39.
4. Louis, D.N., et al., *The 2016 World Health Organization Classification of Tumors of the Central Nervous System: a summary.* Acta Neuropathol, 2016. **131**(6): p. 803-20.
5. Brennan, C.W., et al., *The somatic genomic landscape of glioblastoma.* Cell, 2013. **155**(2): p. 462-77.
6. Stupp, R., et al., *Chemoradiotherapy in malignant glioma: standard of care and future directions.* J Clin Oncol, 2007. **25**(26): p. 4127-36.
7. Ellor, S.V., T.A. Pagano-Young, and N.G. Avgeropoulos, *Glioblastoma: background, standard treatment paradigms, and supportive care considerations.* J Law Med Ethics, 2014. **42**(2): p. 171-82.
8. Weis, S.M. and D.A. Cheresh, *Pathophysiological consequences of VEGF-induced vascular permeability.* Nature, 2005. **437**(7058): p. 497-504.
9. Bao, S., et al., *Glioma stem cells promote radioresistance by preferential activation of the DNA damage response.* Nature, 2006. **444**(7120): p. 756-60.
10. Hegi, M.E., et al., *MGMT gene silencing and benefit from temozolomide in glioblastoma.* N Engl J Med, 2005. **352**(10): p. 997-1003.
11. Jackson, M., F. Hassiotou, and A. Nowak, *Glioblastoma stem-like cells: at the root of tumor recurrence and a therapeutic target.* Carcinogenesis, 2015. **36**(2): p. 177-85.
12. Chiche, J., M.C. Brahimi-Horn, and J. Pouyssegur, *Tumour hypoxia induces a metabolic shift causing acidosis: a common feature in cancer.* J Cell Mol Med, 2010. **14**(4): p. 771-94.
13. Grimm, S.A. and M.C. Chamberlain, *State of the art and perspectives in the treatment of glioblastoma.* CNS Oncol, 2012. **1**(1): p. 49-70.

14. Yang, B., et al., *The ultrastructural difference between CD133-positive U251 glioma stem cells and normal U251 glioma cells.* Ultrastruct Pathol, 2012. **36**(6): p. 404-8.
15. Roos, A., et al., *Molecular and Microenvironmental Determinants of Glioma Stem-Like Cell Survival and Invasion.* Front Oncol, 2017. **7**: p. 120.
16. Hjelmeland, A.B., et al., *Acidic stress promotes a glioma stem cell phenotype.* Cell Death Differ, 2011. **18**(5): p. 829-40.
17. Vescovi, A.L., R. Galli, and B.A. Reynolds, *Brain tumour stem cells.* Nat Rev Cancer, 2006. **6**(6): p. 425-36.
18. Reynolds, B.A. and S. Weiss, *Generation of neurons and astrocytes from isolated cells of the adult mammalian central nervous system.* Science, 1992. **255**(5052): p. 1707-10.
19. Forgac, M., *Vacuolar ATPases: rotary proton pumps in physiology and pathophysiology.* Nat Rev Mol Cell Biol, 2007. **8**(11): p. 917-29.
20. Marshansky, V., J.L. Rubinstein, and G. Gruber, *Eukaryotic V-ATPase: novel structural findings and functional insights.* Biochim Biophys Acta, 2014. **1837**(6): p. 857-79.
21. Toei, M., R. Saum, and M. Forgac, *Regulation and isoform function of the V-ATPases.* Biochemistry, 2010. **49**(23): p. 4715-23.
22. Asgharzadeh, M.R., et al., *Molecular machineries of pH dysregulation in tumor microenvironment: potential targets for cancer therapy.* Bioimpacts, 2017. **7**(2): p. 115-133.
23. McGuire, C., et al., *Regulation of V-ATPase assembly and function of V-ATPases in tumor cell invasiveness.* Biochim Biophys Acta, 2016. **1857**(8): p. 1213-8.
24. Petzoldt, A.G., et al., *Elevated expression of the V-ATPase C subunit triggers JNK-dependent cell invasion and overgrowth in a Drosophila epithelium.* Dis Model Mech, 2013. **6**(3): p. 689-700.
25. Nishi, T. and M. Forgac, *The vacuolar (H+)-ATPases--nature's most versatile proton pumps.* Nat Rev Mol Cell Biol, 2002. **3**(2): p. 94-103.
26. Drose, S., et al., *Inhibitory effect of modified bafilomycins and concanamycins on P- and V-type adenosinetriphosphatases.* Biochemistry, 1993. **32**(15): p. 3902-6.
27. Huss, M. and H. Wieczorek, *Inhibitors of V-ATPases: old and new players.* J Exp Biol, 2009. **212**(Pt 3): p. 341-6.
28. Kinashi, H., K. Someno, and K. Sakaguchi, *Isolation and characterization of concanamycins A, B and C.* J Antibiot (Tokyo), 1984. **37**(11): p. 1333-43.
29. Bowman, E.J., A. Siebers, and K. Altendorf, *Bafilomycins: a class of inhibitors of membrane ATPases from microorganisms, animal cells, and plant cells.* Proc Natl Acad Sci U S A, 1988. **85**(21): p. 7972-6.

30. Kalra, H., et al., *Vesiclepedia: a compendium for extracellular vesicles with continuous community annotation.* PLoS Biol, 2012. **10**(12): p. e1001450.
31. Cocucci, E. and J. Meldolesi, *Ectosomes and exosomes: shedding the confusion between extracellular vesicles.* Trends Cell Biol, 2015. **25**(6): p. 364-72.
32. Al-Nedawi, K., et al., *Intercellular transfer of the oncogenic receptor EGFRvIII by microvesicles derived from tumour cells.* Nat Cell Biol, 2008. **10**(5): p. 619-24.
33. Di Vizio, D., et al., *Oncosome formation in prostate cancer: association with a region of frequent chromosomal deletion in metastatic disease.* Cancer Res, 2009. **69**(13): p. 5601-9.
34. Mondal, A., et al., *Extracellular Vesicles As Modulators of Tumor Microenvironment and Disease Progression in Glioma.* Front Oncol, 2017. **7**: p. 144.
35. Ciardiello, C., et al., *Focus on Extracellular Vesicles: New Frontiers of Cell-to-Cell Communication in Cancer.* Int J Mol Sci, 2016. **17**(2): p. 175.
36. Minciacchi, V.R., M.R. Freeman, and D. Di Vizio, *Extracellular vesicles in cancer: exosomes, microvesicles and the emerging role of large oncosomes.* Semin Cell Dev Biol, 2015. **40**: p. 41-51.
37. Morello, M., et al., *Large oncosomes mediate intercellular transfer of functional microRNA.* Cell Cycle, 2013. **12**(22): p. 3526-36.
38. Gourlay, J., et al., *The emergent role of exosomes in glioma.* J Clin Neurosci, 2017. **35**: p. 13-23.
39. Raposo, G. and W. Stoorvogel, *Extracellular vesicles: exosomes, microvesicles, and friends.* J Cell Biol, 2013. **200**(4): p. 373-83.
40. S, E.L.A., et al., *Extracellular vesicles: biology and emerging therapeutic opportunities.* Nat Rev Drug Discov, 2013. **12**(5): p. 347-57.
41. Yanez-Mo, M., et al., *Biological properties of extracellular vesicles and their physiological functions.* J Extracell Vesicles, 2015. **4**: p. 27066.
42. Nakano, I., et al., *Extracellular vesicles in the biology of brain tumour stem cells--Implications for inter-cellular communication, therapy and biomarker development.* Semin Cell Dev Biol, 2015. **40**: p. 17-26.
43. D'Asti, E., et al., *Oncogenic extracellular vesicles in brain tumor progression.* Front Physiol, 2012. **3**: p. 294.
44. Kucharzewska, P., et al., *Exosomes reflect the hypoxic status of glioma cells and mediate hypoxia-dependent activation of vascular cells during tumor development.* Proc Natl Acad Sci U S A, 2013. **110**(18): p. 7312-7.

45. Ostenfeld, M.S., et al., *Cellular disposal of miR23b by RAB27-dependent exosome release is linked to acquisition of metastatic properties.* Cancer Res, 2014. **74**(20): p. 5758-71.
46. Giusti, I., et al., *From glioblastoma to endothelial cells through extracellular vesicles: messages for angiogenesis.* Tumour Biol, 2016. **37**(9): p. 12743-12753.
47. van der Vos, K.E., et al., *Directly visualized glioblastoma-derived extracellular vesicles transfer RNA to microglia/macrophages in the brain.* Neuro Oncol, 2016. **18**(1): p. 58-69.
48. Winey, M., et al., *Conventional transmission electron microscopy.* Mol Biol Cell, 2014. **25**(3): p. 319-23.
49. Lobb, R.J., et al., *Optimized exosome isolation protocol for cell culture supernatant and human plasma.* J Extracell Vesicles, 2015. **4**: p. 27031.
50. Van Deun, J., et al., *The impact of disparate isolation methods for extracellular vesicles on downstream RNA profiling.* J Extracell Vesicles, 2014. **3**.
51. Witwer, K.W., et al., *Standardization of sample collection, isolation and analysis methods in extracellular vesicle research.* J Extracell Vesicles, 2013. **2**.
52. van der Vlist, E.J., et al., *Fluorescent labeling of nano-sized vesicles released by cells and subsequent quantitative and qualitative analysis by high-resolution flow cytometry.* Nat Protoc, 2012. **7**(7): p. 1311-26.
53. Hendrix, A., et al., *Vacuolar H+ ATPase expression and activity is required for Rab27B-dependent invasive growth and metastasis of breast cancer.* Int J Cancer, 2013. **133**(4): p. 843-54.
54. Kissing, S., et al., *Vacuolar ATPase in phagosome-lysosome fusion.* J Biol Chem, 2015. **290**(22): p. 14166-80.
55. Lotvall, J., et al., *Minimal experimental requirements for definition of extracellular vesicles and their functions: a position statement from the International Society for Extracellular Vesicles.* J Extracell Vesicles, 2014. **3**: p. 26913.
56. Edgar, J.R., et al., *Tetherin is an exosomal tether.* Elife, 2016. **5**.
57. Salerno, M., et al., *Impairment of lysosomal activity as a therapeutic modality targeting cancer stem cells of embryonal rhabdomyosarcoma cell line RD.* PLoS One, 2014. **9**(10): p. e110340.
58. Kulshrestha, A., et al., *Vacuolar ATPase 'a2' isoform exhibits distinct cell surface accumulation and modulates matrix metalloproteinase activity in ovarian cancer.* Oncotarget, 2015. **6**(6): p. 3797-810.

59. Kubisch, R., et al., *V-ATPase inhibition by archazolid leads to lysosomal dysfunction resulting in impaired cathepsin B activation in vivo.* Int J Cancer, 2014. **134**(10): p. 2478-88.
60. McGuire, C., et al., *Regulation of V-ATPase assembly and function of V-ATPases in tumor cell invasiveness.* Biochim Biophys Acta, 2016. **1857**(8): p. 1213-1218.
61. McConnell, M., et al., *Osteoclast proton pump regulator Atp6v1c1 enhances breast cancer growth by activating the mTORC1 pathway and bone metastasis by increasing V-ATPase activity.* Oncotarget, 2017. **8**(29): p. 47675-47690.
62. Di Cristofori, A., et al., *The vacuolar H+ ATPase is a novel therapeutic target for glioblastoma.* Oncotarget, 2015. **6**(19): p. 17514-31.
63. Wiedmann, R.M., et al., *The V-ATPase-inhibitor archazolid abrogates tumor metastasis via inhibition of endocytic activation of the Rho-GTPase Rac1.* Cancer Res, 2012. **72**(22): p. 5976-87.
64. Perez-Sayans, M., et al., *V-ATPase inhibitors and implication in cancer treatment.* Cancer Treat Rev, 2009. **35**(8): p. 707-13.
65. Godlewski, J., et al., *MicroRNA Signatures and Molecular Subtypes of Glioblastoma: The Role of Extracellular Transfer.* Stem Cell Reports, 2017. **8**(6): p. 1497-1505.
66. Xue, M., et al., *Hypoxic exosomes facilitate bladder tumor growth and development through transferring long non-coding RNA-UCA1.* Mol Cancer, 2017. **16**(1): p. 143.
67. Soekmadji, C., et al., *Extracellular vesicles for personalized therapy decision support in advanced metastatic cancers and its potential impact for prostate cancer.* Prostate, 2017.
68. Bandari, S.K., et al., *Chemotherapy induces secretion of exosomes loaded with heparanase that degrades extracellular matrix and impacts tumor and host cell behavior.* Matrix Biol, 2017.
69. Ma, M., et al., *miRNA-221 of exosomes originating from bone marrow mesenchymal stem cells promotes oncogenic activity in gastric cancer.* Onco Targets Ther, 2017. **10**: p. 4161-4171.
70. Figueroa, J., et al., *Exosomes from Glioma-Associated Mesenchymal Stem Cells Increase the Tumorigenicity of Glioma Stem-like Cells via Transfer of miR-1587.* Cancer Res, 2017.
71. Chen, D., et al., *Upregulated exosomic miR23b3p plays regulatory roles in the progression of pancreatic cancer.* Oncol Rep, 2017.
72. Zhang, W., et al., *MicroRNAs in Serum Exosomes as Potential Biomarkers in Clear-cell Renal Cell Carcinoma.* Eur Urol Focus, 2016.

7. SITOGRAPHY

A. http://www.exocarta.org/
B. http://www.microvesicles.org/
C. http://www.evpedia.org/
D. http://c1.accurascience.com/miRecords/
E. http://mirtarbase.mbc.nctu.edu.tw/
F. http://diana.imis.athena-innovation.gr/DianaTools/index.php?r=tarbase/index

8. SCIENTIFIC PRODUCTS

Paper:

-'The vacuolar H+ ATPase is a novel therapeutic target for glioblastomas.' Di Cristofori A., Ferrero S., **Bertolini I.**, Gaudioso G., Russo M.V., Berno V., Vanini M., Locatelli M., Zavanone M., Rampini P., Vaccari T., Caroli M. and Vaira V. Oncotarget, 2015 July.

-'Mitochondrial Akt Regulation of Hypoxic Tumor Reprogramming.' Chae YC, Vaira V, Caino MC, Tang HY, Seo JH, Kossenkov AV, Ottobrini L, Martelli C, Lucignani G, **Bertolini I**, Locatelli M, Bryant KG, Ghosh JC, Lisanti S, Ku B, Bosari S, Languino LR, Speicher DW, Altieri DC. Cancer Cell, 2016 Aug.

* * * * * * * *

Oral communication:

-Oral communication at ISCaM2017 - 4th Annual Meeting - Cancer Metabolism: Exosomes signalling in human glioma stem cells: the central role of V-ATPase proton pump. Bertinoro, October 2017.

-Oral presentation at 1^ YOUNG SCIENTIST WORKSHOP "Stem cell niche: from basic science to clinical application". V-ATPase signaling in glioma. Pavia, May 2016.

* * * * * * * *

Poster:

-Poster presentation at ABCD congress: V-ATPase proton pump regulates exosomes signalling in human glioma stem cells. Bologna, September 2017

-Poster presentation at EAS 2017: “The challanges of optimazing immuno and targeted therapies: from cancer biology to the clinic”: V-ATPase control of exosomes signalling in glioma stem cells.

-Poster presentation at AACR annual meeting 2017: V-ATPase control of EVs signalling in glioma stem cells. Washington, April 2017

-Poster presentation at EMBL Course: “Extracellular Vesicles: from Biology to Biomedical Applications”. V-ATPase & Extracellular Signaling in glioma stem cells. Heidelberg, September 2016.

-Poster presentation at Frontiers in Molecular Biology 2016 SIBBM Seminar “From Single Cell Analysis to Precision Medicine”. V-ATPase signaling in glioma. Naples, June 2016.

* * * * * * * *

Award:

-Best poster award at EMBL Course: "Extracellular Vesicles: from Biology to Biomedical Applications". V-ATPase & Extracellular Signaling in glioma stem cells. Heidelberg, September 2016.

* * * * * * * *

Courses and congresses:

-Novel Solutions for Neural Development and Disease Modeling using primary and iPS cells derived neural cultures – Voden, 26 ottobre 2017

-ISCaM - 4th Annual Meeting - Cancer Metabolism, Bertinoro, 19-21 ottobre 2017

-Nikon worshop @INGM: Spinning disk-video confocal super resolution, INGM, 25-27 settembre 2017

-ABCD congress, 20-24 settembre, Bologna

-EACR-AACR-SIC special conference on the challanges of optimising immuno and target therapies, Firenze, 24-27 giugno 2017

-Sted 3X-3D nanoscopy & light sheet microscopy (DLS), Università di Padova, 7-9 giugno

-AACR annual meeting, Washington DC (USA), 1-5 aprile 2017

-Human Pluripotent Stem Cell (hPSC) Workshop, San Raffaele, 22 marzo 2017

-7th milan meets immunology (MMI) conference, IFOM-IEO, 14 febbraio 2017

-Brain cancer immunotherapy: an update, Istituto Neurologico Besta, 29 novembre 2016

-EMBL Course: "Extracellular Vesicles: from Biology to Biomedical Applications". Heidelberg, Germany, 19-24 September 2016:

-Frontiers in Molecular Biology 2016 SIBBM Seminar "From Single Cell Analysis to Precision Medicine", Naples, Italy, 16-18 June 2016

-1^ YOUNG SCIENTIST WORKSHOP "Stem cell niche: from basic science to clinical application" Pavia, Italy, 8-10 May 2016

-R course, Università dell'Insubria, Busto Arsizio, Italy, November-December 2015

-Medicina di precisione in oncologia, Fondazione IRCCS Istituto Nazionale dei Tumori, Milan, Italy, 25 November 2015

-NGS Data training Course 1 "Intuitive analysis of somatic and germline mutations", Milan, Italy, 29 October 2015

8. ACKNOLOWDGEMENT

This work was supported by Fondazione Cariplo (2014-1148 to Valentina Vaira), Fondazione IRCCS Ca' Granda and Fondazione INGM – Grant in Molecular Medicine 2014 (to VV), and from Ministero della Salute "Ricerca Corrente Program" (to Silvano Bosari and Stefano Ferrero).

Patients' samples were provided by the Neurosurgery Division of Fondazione IRCCS Ca' Granda Ospedale Maggiore Policlinico of Milan after patients' informed consents were signed.

For the contribution in this work, I want to thank:
-my supervisor and co-tutor Valentina Vaira for the opportunity to work in this interesting field and the support during my 3 years of PhD;
-Alessandra Storaci that works with me in the field of V-ATPase proton pump in glioma stem cells and specially because she collected a lot of supernatant and shared with me all the problem of working with ultracentrifugation and extracellular vesicles;
-Andrea Terrasi for the bioinformatics analyses;
-all members of molecular pathology lab, in particular Annamaria Morotti for provide me new ideas and points of view and Ilaria Marangoni and Roberta Tacchi (TB students) that help me during their thesis internship;
-my first tutor Silvano Bosari and my current tutor prof. Stefano Ferrero for the opportunity to work in molecular pathology lab and their support in my formation as a PhD;
-Maria Carla Panzeri (Alembic, San Raffaele) for electron microscopy and immunogold images;
-Valentina Bollati lab (Unimi) for Nanosight analyses.